On the nature of the galactic early-B hypergiants[*]

J. S. Clark[1], F. Najarro[2], I. Negueruela[3], B. W. Ritchie[1], M. A. Urbaneja[4], and I. D. Howarth[5]

[1] Department of Physics and Astronomy, The Open University, Walton Hall, Milton Keynes, MK7 6AA, UK
e-mail: s.clark@open.ac.uk
[2] Departamento de Astrofísica, Centro de Astrobiología, (CSIC-INTA), Ctra. Torrejón a Ajalvir, km 4, 28850 Torrejón de Ardoz, Madrid, Spain
[3] Departamento. de Física, Ingeniería de Sistemas y Teoría de la Señal, Universidad de Alicante, Apdo. 99, 03080 Alicante, Spain
[4] Institute for Astronomy, University of Hawaii, 2680 Woodlawn Drive, Honolulu, Hawaii 96822, USA
[5] Department of Physics & Astronomy, University College London, Gower Street, London, WC1E 6BT, UK

ABSTRACT

Aims. Despite their importance to a number of astrophysical fields, the lifecycles of very massive stars are still poorly defined. In order to address this shortcoming, we present a detailed quantitative study of the physical properties of four early-B hypergiants (BHGs) of spectral type B1-4 Ia$^+$; Cyg OB2 #12, ζ^1 Sco, HD 190603 and BP Cru. These are combined with an analysis of their long-term spectroscopic and photometric behaviour in order to determine their evolutionary status.
Methods. Quantitative analysis of UV–radio photometric and spectroscopic datasets was undertaken with a non-LTE model atmosphere code in order to derive physical parameters for comparison with apparently closely related objects, such as B supergiants (BSGs) and luminous blue variables (LBVs), and theoretical evolutionary predictions.
Results. The long-term photospheric and spectroscopic datasets compiled for the early-B HGs revealed that they are remarkably stable over long periods (≥40 yrs), with the possible exception of ζ^1 Sco prior to the 20th century; in contrast to the typical excursions that characterise LBVs. Quantitative analysis of ζ^1 Sco, HD 190603 and BP Cru yielded physical properties intermediate between BSGs and LBVs; we therefore suggest that BHGs are the immediate descendants and progenitors (respectively) of such stars, for initial masses in the range $\sim$30−60 $M_\odot$. Comparison of the properties of ζ^1 Sco with the stellar population of its host cluster/association NGC 6231/Sco OB1 provides further support for such an evolutionary scenario. In contrast, while the wind properties of Cyg OB2 #12 are consistent with this hypothesis, the combination of extreme luminosity and spectroscopic mass ($\sim$110 $M_\odot$) and comparatively low temperature means it cannot be accommodated in such a scheme. Likewise, despite its co-location with several LBVs above the Humphreys-Davidson (HD) limit, the lack of long term variability and its unevolved chemistry apparently excludes such an identification. Since such massive stars are not expected to evolve to such cool temperatures, instead traversing an O4-6Ia→O4-6Ia$^+$ →WN7-9ha pathway, the properties of Cyg OB2 #12 are therefore difficult to understand under current evolutionary paradigms. Finally, we note that as with AG Car in its cool phase, despite exceeding the HD limit, the properties of Cyg OB2 #12 imply that it lies below the Eddington limit – thus we conclude that the HD limit does not define a region of the HR diagram inherently inimical to the presence of massive stars.

Key words. stars: evolution – stars: early-type – supergiants – stars: fundamental parameters – stars: mass-loss

1. Introduction

Very massive stars are of considerable astrophysical interest given their role in driving galactic evolution via the copious production of ionising radiation and the deposition of chemically processed material and mechanical energy into the interstellar medium. They are thought to be the progenitors of Type Ibc and II supernovae (SNe) and, in low metallicity environments, gamma ray bursts (GRBs). The diverse nature of their core collapse SNe is also mirrored in the nature of their relativistic remnants which, for a given progenitor mass, may be either a neutron star or black hole depending on their pre-SNe (binary mediated?) mass loss history (e.g. Ritchie et al. 2010). Moreover, with $M_V \sim -11$ during particular phases of their post-main sequence evolution, they have the potential to probe the distance to – and chemical composition and star formation history of – external galaxies out to distances of $\sim$10 to 30 Mpc

with the current and next generation of ground based telescopes (Kudritzki 2010).

Unfortunately, despite considerable theoretical efforts (e.g. Meynet & Maeder 2005; Heger et al. 2000) we currently lack a comprehensive theoretical framework to fully understand and exploit all aspects of these stars; a problem compounded by comparatively weak observational constraints on a number of key physical processes that drive massive stellar evolution, such as the influence of (metallicity dependent) mass loss, the role of rotational mixing and the effect of binary interactions. In this regard, a critical test of evolutionary theory is the accurate reproduction of the properties of stars within the short lived transitional phase between the main sequence (MS) and H-depleted Wolf-Rayets (WRs), which is populated by a diverse "zoo" of disparate objects such as blue and yellow hypergiants (B/YHGs) and luminous blue variables (LBVs)/P-Cygni supergiants. For example, a crucial observational finding that must be replicated is the apparent dearth of cool evolved stars at high luminosities (the empirical Humphreys-Davidson (HD) limit; Humphreys & Davidson 1979); in this regard the YHG/RSG populations of

---

M 31 (Drout et al. 2009) and the Galactic cluster Westerlund 1 (Clark et al. 2010) already pose problems for current theoretical models.

Another manifestation of this uncertainty is an inability to incorporate the various members of the post-MS "zoo" into a coherent evolutionary scheme as a function of initial stellar mass. Various authors (e.g. Langer et al. 1994; Crowther et al. 1995; Martins et al. 2007, 2008) have proposed scenarios which have increasingly been informed by quantitative non-LTE model atmosphere analysis of different stellar populations, latterly located within coeval young massive Galactic clusters. In order to build on this approach we present an analysis of the properties of the BHGs of early B spectral type, which hitherto have escaped systematic study.

The Ia$^+$ luminosity class was first applied to a group of four highly luminous ($M_V < -8$) B "super-supergiants" within the LMC by Keenan (1971), which were later described as "hypergiants" by van Genderen et al. (1982). These are further distinguished from normal BSGs by the presence of (P Cygni) emission in the Balmer series (cf. HD 190603; Lennon et al. 1992). Currently, to the best of our knowledge only 16 (candidate) BHGs have been identified within the Galaxy, of which eight are of early (≤B4) and eight of late (≥B5) spectral type; these are summarised in Table 1. Of the early BHGs, Kaper et al. (2006) have already presented the results of a quantitative analysis of BP Cru (=Wray 977; the mass donor in the High Mass X-ray Binary GX301-2); in this paper we present the result of equivalent analyses of Cyg OB2 #12, ζ^1 Sco(=HD 152236) and HD 190603. Foreshadowing Sect. 4, while the latter two objects have previously been subject to similar studies (e.g. Crowther et al. 2006; Searle et al. 2008), we employ more extensive multi-wavelength datasets that enable significantly more accurate determinations of physical parameters; for example the lack of wind contamination in the higher Balmer and Paschen lines sampled here permitting a more robust determination of the surface gravity. Insufficient data exist to undertake comparable modeling of the remaining early B hypergiants, although we are currently in the process of obtaining the requisite observations.

Of these stars, Cyg OB2 #12 is of particular interest as it has long been recognised as one of the intrinsically brightest, and potentially most luminous stars in the Galaxy (=Schulte 12; Sharpless 1957; Schulte 1958), lying well above the HD limit and so should provide a stringent test of current evolutionary theory. Moreover, BHGs have previously been associated with the LBV phenomenon by various authors (e.g. Clark et al. 2005a) and LBVs in turn have been implicated as both critical to the formation of WRs and as the immediate precursors of type II SNe (Smith & Conti 2008). Finally, Cyg OB2 #12 and ζ^1 Sco are generally thought to be located within the Cyg OB2 and Sco OB1 associations respectively, which have both benefited from multiple (recent) studies[1] and hence in principal should help in the assessment of both the nature of their progenitors as well as their placement in a post-MS evolutionary sequence.

The paper is structured as follows. In Sect. 2 we briefly detail the new observations of the 3 BHGs analysed in this work (Cyg OB2 #12, ζ^1 Sco and HD 190603; we utilise the dataset and analysis of Kaper et al. (2006) for BP Cru), while summarising the consolidated observational datasets in Sect. 3. This enables us to assess the degree of short and long-term variability

demonstrated by the program stars as well as providing the spectra and optical-radio spectral energy distributions (SEDs) for the non-LTE model atmosphere quantitative analysis. The results of this are presented in Sect. 4, discussed in Sect. 5 and conclusions presented in Sect. 6. Finally, an extensive summary of the (historical) observational properties of Galactic BHGs is documented in Appendix A, the spectropolarimety of Cyg OB2 #12 and ζ^1 Sco discussed in Sect. 4 is presented in Appendix B and Appendix C contains an analysis of the properties of the host cluster (NGC 6231) and association (Sco OB1) of ζ^1 Sco.

2. Observations and data reduction

In order to accomplish the goals of the paper we have compiled extensive datasets for Cyg OB2 #12, ζ^1 Sco and HD 190603, utilising both new and published observations. A full presentation of the data for these (and other) BHGs may be found in Appendix A, while we briefly describe the new observations undertaken and data reduction employed below. In Appendix B we also present the results of analysis of previously unpublished spectropolarimetric observations of Cyg OB2 #12 and ζ^1 Sco; while these are not directly employed in the quantitative modeling of these stars they serve as a useful check on the geometry of the cirumstellar environment of these stars.

2.1. Cyg OB2 #12

New high resolution and S/N spectra of Cyg OB2 #12 were obtained through the *William Herschel* Telescope (WHT) service programme on 2008 July 28, employing the ISIS double-beam spectrograph equipped with the R1200B and R1200R gratings; a summary of the resultant wavelength ranges is given in Table 2. These observations were supplemented with a further five epochs of previous unpublished archival observations dating from 1992–2007; these too are summarised in Table 2. All spectra were reduced in a consistent manner using the Starlink packages Figaro and Kappa, with selected regions presented in Figs. 1, 2 and A.1. Continuum normalisation was accomplished via spline fitting and division, yielding uncertainties of a few percent at most. Likewise, the RMS on the fits to the arc spectra are of the order of ~0.03 pixels, resulting in a negligible error for wavelength callibration.

Unfortunately the distance and reddening to Cyg OB2 #12 preclude UV observations, so the 4000–9000 Å spectrum obtained in 2008 formed the primary dataset employed in this study. This was supplemented with the 1 μm spectrum of Conti & Howarth (1999), which encompasses the important He I 1.083 μm transition, as well as the flux callibrated ISO-SWS spectrum presented by Whittet et al. (1997) and an archival *Spitzer* Space Telescope IRS spectrum (Houck et al. 2004). An optical – radio spectral energy distribution (SED) was constructed from continuum flux measurements from the literature (Tables A.1−A.3). While these observations were not contemporaneous, as demonstrated in Sect. A.1 there is no evidence for substantial variability/evolution over the timeframe spanned by these observations. Hence we are confident that such an approach is well justified and this is supported a posteriori by the excellent fits to the combined dataset.

2.2. ζ^1 Sco

A total of 18 new spectra have been utilised for the analysis of the long-term behaviour of ζ^1 Sco. Unpublished

---

[1] E.g. Cyg OB2: Massey & Thompson (1991), Knödlseder (2000), Comerón et al. (2002), Hanson (2003) & Negueruela et al. (2008) and Sco OB1: Reipurth (2008), Sana et al. (2006a, 2007; 2008) and Raboud et al. (1997).
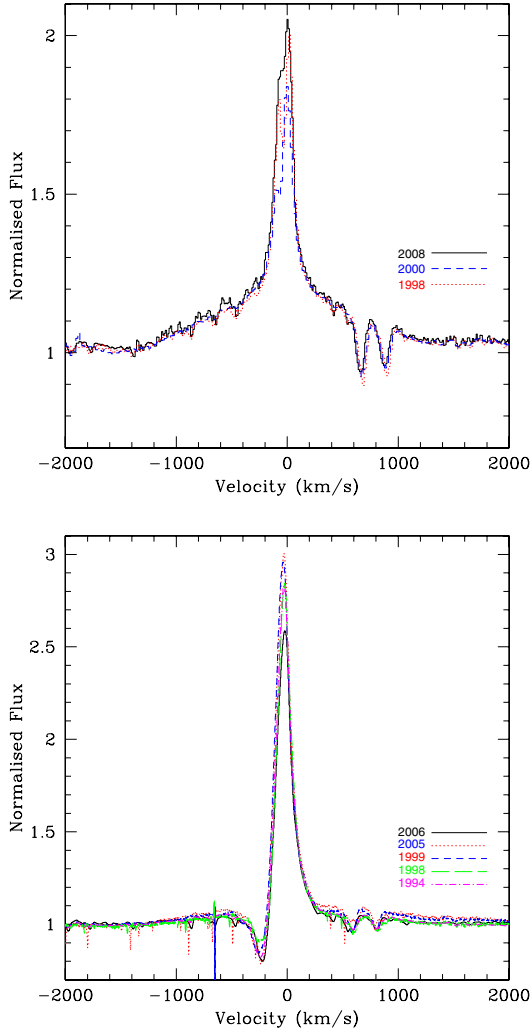
Fig. 1. Comparison of three (1999–2008) and five (1994–2009) epochs of Hα observations for Cyg OB2 #12 (*upper panel*) and ζ^1 Sco (*lower panel*) demonstrating line profile variability at low projected velocities. Note the corresponding lack of variability in the line wings and the C $\textsc{ii}\lambda\lambda$ 6578, 6582 doublet in the red wing. Due to their lower resolution, spectra of Cyg OB2 #12 from 1992+5 are not presented, but are consistent to these spectra when all are convolved to a matching resolution.

ESO 2.2 m/FEROS spectra from 1998-9 (Program ID 063.H-0080; PI: Kaufer) and 2005 (Program ID 075.D-0103(A); PI:Dufton) were kindly provided by Otmar Stahl (2010, priv. comm.) and Phillip Dufton (2010, priv. comm.) respectively. Data reduction was accomplished via the custom pipeline described in Stahl et al. (1999). Continuum normalisation was accomplished by first dividing the spectra by the instrumental response curve, with a subsequent division by a spline function; as before, the errors in this procedure are of the order of a few percent. The spectrum from 2006 February 17 was obtained by us with the ESO NTT/EMMI; standard reduction procedures were employed and are discussed in Negueruela et al. (in prep.). Finally new blue and red end spectra from 2009 March 06 were obtained from the ESO archive (Program ID 082.C-0566(A); PI: Beletsky). These were obtained with the VLT/UVES with cross disperser gratings CD1, 2 and 3 and were reduced using the standard ESO pipeline. A full summary of these new observations is provided in Table 2 and selected spectra are presented in Figs. 1, 2 and A.1. The full dataset used for modeling also in-
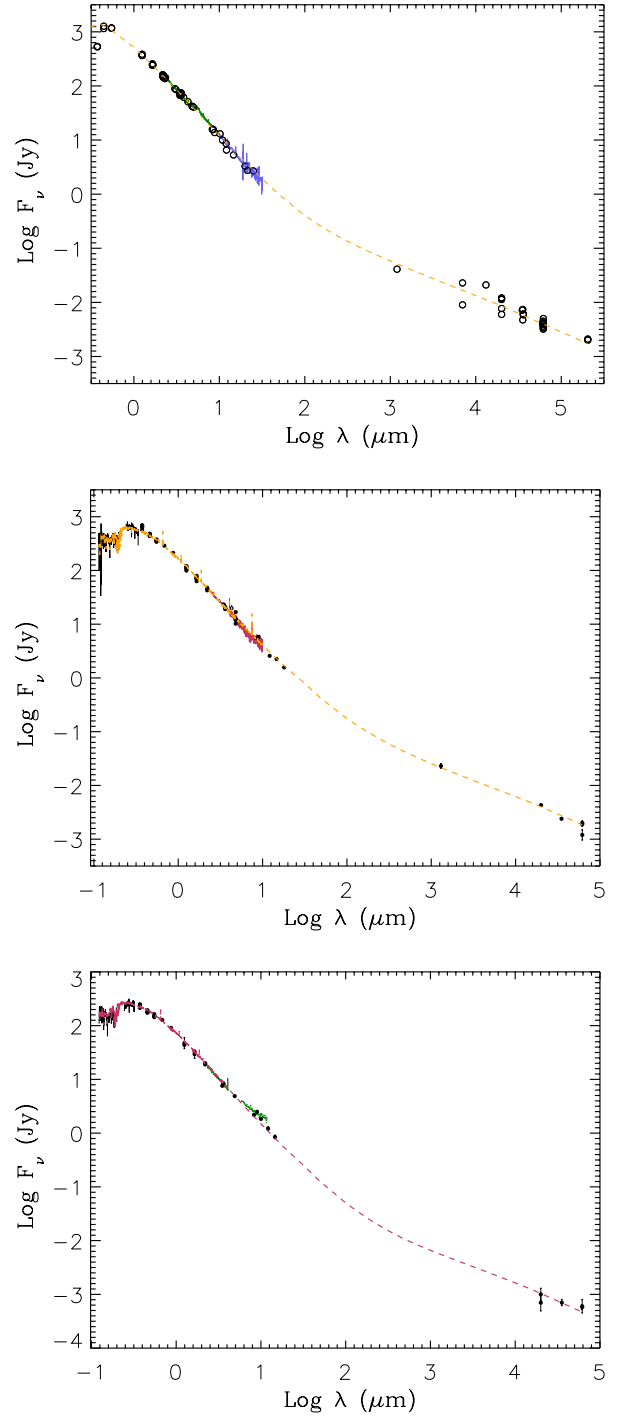

Fig. 2. Comparison of synthetic spectra (yellow dashed line) with the optical to radio SEDs of Cyg OB2 #12 (*top panel*), ζ^1 Sco (*middle panel*) and HD 190603 (*bottom panel*). Note the lack of a near-mid IR excess signalling the absence of significant amounts (warm) circumstellar dust. Physical parameters employed in the modeling – such as L_{bol} and $E(B-V)$ – may be found in Table 4 and Sects. 4.1 and 4.2.

cludes archival IUE and ISO spectra, as well as published photometry summarised in Tables A.1−A.3.

2.3. HD 190603

Finally, we make use of solely archival data for the quantitative analysis of HD 190603. As with the other objects, the sources of data used in constructing the SED are given in Tables A.1−A.3. Spectroscopic data were taken from Lennon

et al. (3950–5000 Å+ Hα; 1992), Rivinius et al. (4050–6800 Å; 1997), Andrillat et al. (8390–8770 Å) as well as one from the IACOB database (3710–6800 Å; Sergio Simón-Díaz 2011, priv. comm.).

3. The observational properties of BHGs

BHGs form a spectroscopically homogeneous class of objects that are distinguished from BSGs by the presence of Balmer emission lines. However, they have been implicated in the LBV phenomenon (Sect. 1) and so it is of interest to compare their 0.4–4.1 μm spectra with those of bona fide LBVs in both hot and cool phases. Suitable comparison spectra across this wavelength range are provided by, amongst others, Stahl et al. (2001), Hillier et al. (1998), Groh et al. (2007), Clark et al. (2003a, 2009, 2011) and Lenorzer et al. (2002). Significant differences are evident; specifically the weakness of the H I and He I lines in the BHG spectra, as well as the absence of emission in low excitation metallic lines such as Fe II and III that characterise the spectra of LBVs.

A second observational characteristic of *some* LBVs is the presence of circumstellar dust – indeed the presence of a detached circumstellar nebula has been advanced to support the LBV nature of the late-B hypergiant HD 168625. Of the early BHGs in question, only BP Cru is known to show evidence for warm dust (e.g. Fig. 2; Moon et al. 2007), although with $M_{\rm dust} \sim 5.2 \times 10^{-8}~M_\odot$, considerably less than is associated with either LBVs or supergiant B[e] stars (Egan et al. 2002; Clark et al. 2003a; Kastner et al. 2006).

However, the defining characteristic of LBVs is their dramatic spectroscopic and photometric variability over timescales of months–years. Motivated by reports of spectral variability amongst both early- and late-B HGs we undertook an exhaustive literature search for these objects, which we present in Appendix A, and briefly discuss here. As highlighted by previous authors, there is strong observational evidence for a physical association between LBVs and low-luminosity, late-B HGs such as HD 160529 and HD 168607; however, the link is far from proven for earlier, more luminous BHGs. Owing to their luminosities extensive spectroscopic and photometric datasets exist for such stars, with the majority extending back to the mid-20th century, for Cyg OB2 #12 and HD 190603 to the turn of last century and (sparse) photometric data for ζ^1 Sco potentially many centuries before that (Appendix A)[2].

Cyg OB2 #12 has long been suspected of being spectroscopically variable, being variously classified as B3-8 Ia$^+$ in the literature (e.g. Table A.4 and refs. therein). However, upon close examination of the spectra and classification criteria employed, we conclude that long-term evolution of the stellar *temperature* between 1954–2008 is probably absent (Appendix A.1.2) and that the reports of such behaviour result from comparison of low S/N and resolution spectra and, crucially, the sensitivity of the commonly employed He II 4471/Mg II 4481 criterion to the properties of the photosphere/wind transition zone *as well as photospheric temperature* (Sect. 4.1). This conclusion is bolstered by the lack of secular photospheric variability dating back to the 1890s, although low level, apparently aperiodic variability does appear present (e.g. Gottlieb & Liller 1978).

---

[2] Unfortunately, in many cases early observations are presented in the literature without precise observational dates. Nevertheless, the similarity of these data to more recent observations supports the lack of long term variability in such cases.
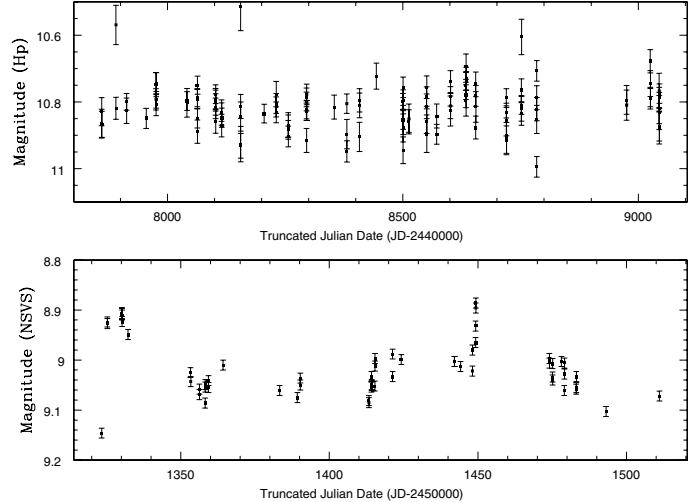
Fig. 3. HIPPARCOS (*top panel*: 1989–1993) and NSVS (*bottom panel*: 1999–2000) lightcurves of Cyg OB2 #12. Both panels plot the (non standard) instrumental magnitudes (references to these are provided in the text) and we caution that the scale of both axes differ between the two panels.

Based on the datasets discussed in Appendix A, similar conclusions may be drawn for the remaining early- (BP Cru, HD 80077, HD 190603, HD 168454, Wd1-5 and 13) and mid-B HGs (Wd1-7 and 33), with the potential exception of ζ^1 Sco. Spectroscopically, it is the best sampled of all the BHGs and shows no evidence for evolution between ~1891–2009 (Table A.5). Likewise, it appears to have remained photometrically stable since at least 1949 (Table A.1), although isolated historical photometric observations dating back many centuries are available in the literature, from which Sterken et al. (1997) infer possible LBV like variability in the 18–19th century.

However, while long-term variability appears rare or absent amongst the early-B HGs, rapid (~day to day) line profile variability (LPV) in both wind dominated emission and photospheric absorption lines appears ubiquitous, persistent and well documented (e.g. Fig. 1 and Appendix A and references therein). These behaviours are thought to arise from time variable wind structure and photospheric pulsations respectively, with the former also potentially giving rise to variable radio continuum emission (e.g. González & Cantó 2008), although changes in the the degree of ionization of the wind are another possible cause of this phenomenon.

Likewise, rapid, low amplitude photometric variability is present amongst all the BHGs (e.g. Fig. 3 and Appendix A). Such behaviour has long been recognised as being characteristic of luminous stars of all spectral types (the "α Cygni" variables; e.g. Burki 1978; van Leeuwen et al. 1998; Clark et al. 2010) and again is typically attributed to photospheric pulsations.

We conclude that the temporal behaviour of the early-B HGs appears entirely typical of the wider population of luminous, early-spectral-type non-LBV stars, with the potential exception of ζ^1 Sco in the 18–19th centuries and a possible sudden $\Delta m_{\rm B} \sim 0.4$ mag "glitch" in the lightcurve of Cyg OB2 #12 in the mid-1940s (Gottlieb & Liller 1978).

4. Quantitative modeling

In order to more fully address the physical properties of Cyg OB2 #12, ζ^1 Sco and HD 190603 we have employed the

Table 1. Summary of Galactic BHG properties.

Star	Spectral type	Co-ordinates		V band (mean)	Cluster/ association
		RA	Dec.		
BP Cru	B1 Ia$^+$	12 26 37.56	−62 46 13.2	10.68	–
HD 169454	B1 Ia$^+$	18 25 15.19	−13 58 42.3	6.65	–
ζ^1 Sco	B1.5 Ia$^+$	16 53 49.73	−42 21 43.3	4.78	Sco OB1
HD 190603	B1.5 Ia$^+$	20 04 36.17	+32 13 07.0	5.66	–
HD 80077	B2.5 Ia$^+$	09 15 54.79	−49 58 24.6	7.57	Pismis 11
Cyg OB2 #12	B3-4 Ia$^+$	20 32 40.96	+41 14 29.3	11.47	Cyg OB2
Wd1-5	WNL/B Ia$^+$	16 46 02.97	−45 50 19.5	17.49	Wd1
Wd1-13	WNL/B Ia$^+$	16 47 06.45	−45 50 26.0	17.19	Wd1
Wd1-7	B5 Ia$^+$	16 46 03.62	−45 50 14.2	15.57	Wd1
Wd1-33	B5 Ia$^+$	16 47 04.12	−45 50 48.3	15.61	Wd1
HD 183143	B7 Iae	19 27 26.56	+18 17 45.2	6.92	–
HD 199478	B9 Iae	20 55 49.80	+47 25 03.6	5.73	–
HD 168625	B8 Ia$^+$	18 21 19.55	−16 22 26.1	8.44	–
Wd1-42a	B9 Ia$^+$	16 47 03.25	−45 50 52.1	–	Wd1
HD 168607	B9 Ia$^+$	18 21 14.89	−16 22 31.8	–	–
HD 160529	B8-A9 Ia$^+$	17 41 59.03	−33 30 13.7	–	–

Notes. No *V*-band magnitude is available for Wd1-42a, while both HD 168607 and 160529 are known large amplitude photometric variables (Sect. A.6).

Table 2. Summary of unpublished spectral observations.

Date	Telescope	Wavelength range (Å)	Resln.
Cyg#12			
1992 July 17	INT	4036–4836	4000
		5765–9586^a	4000
1995 July 17	WHT	6172–6980	4000
1998 Aug. 09	WHT	3940–5737	8000
		6366–6772	8000
2000 July 17	INT	3940–5737	8000
		6327–6727	8000
2007 Aug. 22	WHT	7600–8900	10 000
2008 July 22	WHT	4000–4700	4500
		4500–5270	4500
		6450–7150	7000
		8350–8900	10 000
ζ^1 Sco			
1998 October 7	ESO 2.2-m	4000–8950^b	48 000
1999 July–Aug.	ESO 2.2-m^c	4000–8950^b	48 000
2005 April 24	ESO 2.2m	3800–6800	48 000
2006 February 17	NTT	3933–7985	9840
2009 March 06	VLT	3060–5600	

Notes. $^{(a)}$ This wavelength coverage was obtained via 5 overlapping observations. $^{(b)}$ Approximate usable wavelengths. $^{(c)}$ 14 spectra obtained between July 17 to August 4.

non-LTE model atmosphere code CMFGEN (Hillier & Miller 1998, 1999). This solves the radiative-transfer equation for a spherically symmetric wind in the co-moving frame under the constraints of radiative and statistical equilibrium. Since the code does not solve for the wind structure from first (physical) principles, a velocity structure must be chosen; we adopted a standard β-type law[3]. Given the relatively high wind densities of BHGs, the role of the hydrostatic structure and the transition region between photosphere and wind becomes crucial to interpret the spectra (e.g. Sect. 4.1 and Fig. 8). Because of this, we used a hydrostatic density structure at depth (the "pseudo-photosphere") matched to a β-law wind, requiring the density to be continuous at the transition. The location of the transition is fixed by the adopted base velocity of the wind, $v_{\rm phot}$ (a free parameter in the fitting), which specifies the density through the equation of mass continuity. This approach is similar to that of, e.g., Santolaya-Rey et al. (1997), except that in our implementation the flux-weighted mean opacity is used in preference to the Rosseland mean opacity Several comparisons using "exact" photospheric structures from TLUSTY (Hubeny & Lanz 1995) showed excellent agreement with our method[4].

The main atomic processes and data sets are discussed in Hillier & Miller (1998, see Dessart & Hillier 2010 for an updated description of the atomic data). The list of model atoms utilized in our calculations is provided in Table 3, including for each ion the number of super and full levels and number of bound-bound transitions. The CMFGEN model is then prescribed by the stellar radius, R_*, the stellar luminosity, L_*, the mass-loss rate, $\dot{M}$, the velocity field, $v(r)$ (defined by β, $v_{\rm phot}$ and the terminal velocity, v_∞), the volume filling factor, f, characterizing the clumping of the stellar wind, and elemental abundances. The interstellar reddening parameters $E(B-V)$ and R_V are also obtained by fitting the model SEDs to the available photometric data. Finally, the equatorial rotation velocity, $v_e \sin i$, and the atmospheric macroturbulent velocity, $v_{\rm macro}$, were estimated in Fourier space (Simón-Díaz & Herrero 2007) from a selected sample of photospheric lines.

Given the number of free parameters required to specify a fit it is not possible to survey the full parameter space systematically in order to establish robust error estimates; hence errors quoted in this paper represent the range of values for which an acceptable fit to the data may be obtained. Nevertheless, we discuss error estimates for key parameters for each of the stars analysed below. The validity of this technique has been demonstrated by calibration to stars of similar temperature and luminosity for

---

[3] The β-type law is given by $v(r) = v_\infty \times (1 - b/r)^\beta$, where $b = r_{\rm phot} \times (1 - (v_{\rm phot}/v_\infty)^{(1/\beta)})$ and $r_{\rm phot}$ and $v_{\rm phot}$ are the radius and velocity at the connection point between the β-law and the hydrostatic structure.

[4] The latest version of CMFGEN, which allows the user to compute the exact hydrostatic structure, showed full consistency with our method. At this stage, we prefer our approach as it allows for more flexibility to study the crucial transition region.

Table 3. Model atoms included in our calculations.

Species	# Full levels	# Super levels	# Of transitions
H I	30	30	435
He I	59	59	592
He II	5	5	10
C II	80	45	648
C III	38	22	149
C IV*	8	5	22
N I	63	25	344
N II	179	86	1936
N III	20	11	61
O I	75	23	450
O II	102	46	992
Na I	44	18	345
Mg II	50	37	597
Al II	20	12	41
Al III	45	17	362
Si II	72	35	491
Si III	83	47	532
Si IV	28	17	129
S II	85	26	745
S III	63	31	331
Ca II	32	25	157
Cr III	209	36	2444
Cr IV	242	30	4732
Fe II	709	233	18 011
Fe III	812	87	21 383
Fe IV	417	62	8353
Ni II	254	33	3354
Ni III	336	34	5181
Ni IV	294	56	4174
Total	4160	1137	72 827

Notes. [*] Not used in Cyg OB2 #12.

which UV, optical and near-IR data were available (Najarro et al. 1999; Najarro 2001).

A comparison of the predicted SEDs to our data for the three stars is presented in Fig. 2, while selected regions of the synthetic spectra are overplotted on the observed 4090−11 050 Å spectrum of Cyg OB2 #12 in Fig. 4, the UV-near IR (∼1200−22 100 Å) spectrum of ζ^1 Sco in Figs. 5 and 6 and the optical (∼4000−7000 Å) spectrum of HD 190603 in Fig. 7. The optical data shown in Fig. 6 correspond to the 2006 ESO EMMI/NTT run. Fits to the earlier FEROS spectra supplied by Otmar Stahl – which provide a more extended wavelength coverage – are shown in Fig. D.1. The latter were used to obtain the final stellar properties as they encompass the high Balmer and Paschen lines which constrain the surface gravity. A summary of the results of the analyses for the 3 stars is presented in Table 4, along with the parameters of the B1 Ia$^+$ star BP Cru, obtained via an identical methodology by Kaper et al. (2006).

4.1. Cyg OB2 #12

For the purposes of modeling Cyg OB2 #12 we employed the dataset described in Sect. 3 and Appendix A. We have also assumed membership of Cyg OB2 and hence a distance, $d \sim$ 1.75 kpc (e.g. Negueruela et al. 2008 and refs. therein); we return to this issue below.

Temperature, gravity and luminosity The available optical and NIR spectra allowed us to make use of several ionization

equilibria to estimate the effective temperature, and thus constrain the ionization structure of Cyg OB2 #12. Hence, we were able to utilize simultaneously Si III/Si II, O II/O I, N II/N I and Fe III/Fe II line ratios. The S III/S II equilibrium was only used for a consistency check, as the weak diagnostic S III 4253 Å line suffers from a poorer S/N ratio in the blue spectral region due to reddening. We refer the reader to Sect. A.1.2 for a detailed description of the available diagnostic lines.

When analyzing the ionization equilibria, we found that while lines belonging to higher ionization stages react sensitively to effective temperature and to lesser extent to gravity, those corresponding to the lower ionization stage display a high sensitivity not only to temperature and gravity, but also the location of the transition region between photosphere and wind, characterised by v_{phot} (especially the Si II, Fe II and O I lines). This sensitivity is clearly illustrated in Fig. 8 (right panel), where the choice of v_{phot} significantly affects the resulting strength of the Fe II 5170 Å line, leaving the Fe III lines basically unaffected. Thus, if a lower transition velocity is chosen, a lower effective temperature is required to match the Fe III/Fe II ratio. As we will show later, this effect is responsible for our somewhat lower T_{eff} values when compared to other studies (see Sect. 4.2). Interestingly, Fig. 8 (left panel) also shows how the ratio of the diagnostic lines He I 4471 and Mg II 4481 Å, which are used for spectral typing, also shows a moderate dependence on the transition region. Thus, a model with $v_{phot} = 0.5v_{sound}$ will yield equally strong He I 4471 and Mg II 4481 Å, while if the transition takes place at $v_{phot} = 0.05v_{sound}$, He I 4471 Å clearly becomes stronger than Mg II 4481 Å.

We note that this moderate dependence on the transition region becomes important in BHGs, due to the presence of a strong, dense wind and should be negligible in B supergiants, where the absorption lines will form in deeper photospheric layers that are largely unaffected by the photosphere-wind transition region. Therefore, despite the large number of diagnostics, our final estimate of the effective temperature, ($T_{eff} = 13.7$ kK, see Table 4) is subject to a moderate uncertainty. We find +800 K and –500 K as upper and lower error bounds.

Once the effective temperature was obtained, and assuming a distance of $d \sim 1.75$ kpc, we proceeded to fit the observed SED of Cyg OB2 #12 from the optical through radio (see Fig. 2) and hence derived the reddening, stellar radius and, therefore, the stellar luminosity. We found $E(B - V) = 3.84$ and a reddening parameter $R_V = 2.65$, corresponding to $A_V = 10.18$. This value shows excellent agreement with the $A_V = 10.20$ found by Torres et al. 1991, although they obtained a higher total to selective extinction parameter ($R_V = 3.04$)

From these values we obtained a stellar radius of 246 $R_\odot$ and a final luminosity of 1.9×10^6 $L_\odot$. The temperature and resultant luminosity are broadly comparable to previous qualitative studies (e.g. Massey & Thompson 1991; Hanson 2003), confirming that it is an extraordinarily luminous, but comparatively cool BHG.

The Paschen lines in the *I* Band provide the best constraints for the surface gravity, especially the run of the line overlap among the higher members (Fig. 4). Compared to the classical optical diagnostic lines – Hγ and Hδ – the higher Paschen series lines are significantly less affected by the stellar wind (and consequently clumping) and the wind/photosphere transition region. Nevertheless, the influence of the latter once again translates into a larger uncertainty in the (lower) error. Thus, we find $\log g = 1.70^{+0.08}_{-0.15}$, corresponding to a spectroscopic mass of $M = 110^{+23}_{-31}$ $M_\odot$.
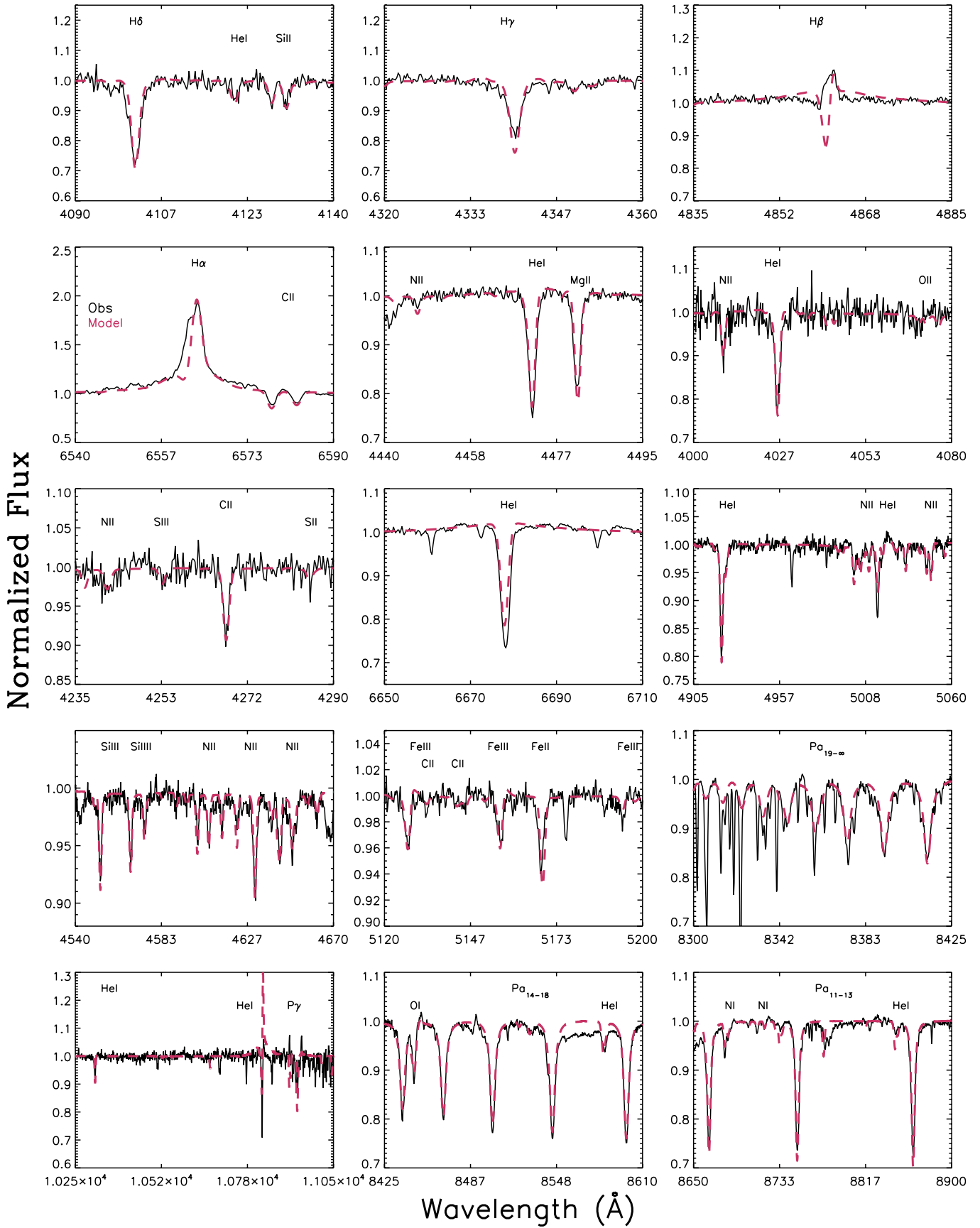
Fig. 4. Comparison of the synthetic spectrum of Cyg OB2 #12 (red dashed line) with observational data for various transitions between 4090–11 050 Å. Note that the narrow absorption lines which have not been labeled are telluric in origin.

Table 4. Model parameters for the BHGs Cyg OB2 #12, ζ^1 Sco, HD 190603 & BP Cru (upper panel) and Galactic B *supergiant* comparison (lower panel; Searle et al. 2008).

Star	Spec. type	DM	M_V	$\log(L_*)$ $L_\odot$	R_* $R_\odot$	$T_{\rm eff}$ kK	$\dot{M}$ $10^{-6}\,M_\odot\,{\rm yr}^{-1}$	v_∞ km s^{-1}	β	f	$\log g$	M_* $M_\odot$
Cyg OB #12	B3-4	11.21	−9.85	6.28	246.0	13.7	3.0	400	3.0	0.04	1.70	110
ζ^1 Sco	B1.5	11.07	−8.50	5.93	103.0	17.2	1.55	390	2.25	0.06	1.97	36
		11.50	−8.93	6.10	125.5	17.2	2.07	390				53
HD 190603	B1.5	10.98	−7.53	5.58	63.0	18.0	1.09	485	2.25	0.25	2.10	18
		12.38	−8.93	6.14	120.0	18.0	2.87	485				65
BP Cru	B1	12.41	−7.47	5.67	70.0	18.1	10.0	305	2.25	1.0	2.38	43
	B1			5.44	36.5	22.0					2.41	12
	B1.5			5.44	44.5	19.9					2.41	18
	B3			5.37	60.4	16.4					2.16	19
	B4			5.34	63.5	15.8					2.06	16

Star	Spec type	$v_{\rm turb}$ km s^{-1}	$v_e \sin i$ km s^{-1}	$v_{\rm macro}$ km s^{-1}	$\frac{v_{\rm phot}}{v_{\rm sound}}$	H/He	N/N$_\odot$	C/C$_\odot$	O/O$_\odot$
Cyg OB #12	B3-4	12.5	38	50	0.02	10	2.7	0.21	0.55
ζ^1 Sco	B1.5	12.5	45	50	0.5	5	5.5	0.33	0.32
HD 190603	B1.5	15	49	55	0.5	5	5.5	0.33	0.40
BP Cru	B1	10	55	–	0.5	3.5	4.8	2.0	0.40

Notes. R_* corresponds to $R(\tau_{\rm Ross} = 2/3)$, the H/He ratio is given by number and $v_{\rm phot}$ in terms of $v_{\rm sound}$. Abundances are relative to solar values from Anders & Grevesse (1989) and have uncertainties of, typically, ~0.2 dex; if we use the values from Asplund et al. (2006) as a reference the derived ratios need to be scaled by 1.49, 1.86 and 1.86 for C, N and O respectively. The results presented here assume a distance of 1.75 kpc for Cyg OB2 #12 ($DM = 11.21$). Apart from the assumed distance of 1.64 kpc for ζ^1 Sco ($DM = 11.07$, Sana et al 2006) we also provide corresponding stellar properties for the other distance estimate (1.99 kpc, $DM = 11.50$) assumed in previous spectroscopic studies. For HD 190603 we display the stellar properties assuming a distance of 1.57 kpc ($DM = 10.98$) as well as those which would result if the object had the same M_V as ζ^1 Sco. Finally a distance of 3.04 kpc (Kaper et al. 2006) is assumed for BP Cru.

Wind properties and clumping Unfortunately, the moderate reddening affecting Cyg OB2 #12 prevents us from securing UV observations from which one might derive firm v_∞ estimates. Furthermore, as with ζ^1 Sco and HD 190603, Cyg OB2 #12's stellar wind is not sufficiently dense that alternative v_∞ diagnostic lines such as Hα or He I 10 830 Å can reach their full potentiallity and unambiguously yield the wind terminal velocity.

Highlighting this difficulty, Souza & Lutz (1980) suggested a terminal velocity of 1400 km s^{-1}, based on the presence of a blueshifted absorption feature in the Hα profile; a value which was subsequently used to obtain the mass-loss rate from radio (Abbott et al. 1981) and IR measurements (Leitherer et al. 1982). Subsequently, Klochkova & Chentsov (2004) revised the estimate of the wind's terminal velocity significantly downwards. Based on higher resolution Hα observations they identified strong electron scattering wings extending up to 1000 km s^{-1}, as well as blueshifted absorption up to ~160 km s^{-1} which they attributed to the wind's true v_∞. However our models indicate that this blueshifted feature *does not directly reflect* v_∞ but rather results from the run of the density and ionization structures within the wind which shapes Hα.

This is shown in Fig. 9, where models with v_∞ ranging from 400 to 1000 km s^{-1} yield an absorption feature around 100–200 km s^{-1} to the blue of Hα in the resultant synthetic spectra. Moreover, values of v_∞ significantly below 400 km s^{-1} appear too low to reproduce the high velocity line emission while, depending on the normalization errors of the Hα profile, values between 400 and 1000 km s^{-1} are potentially consistent. We also found that the blue absorption component of the He I 10 830 Å line is likewise not able to distinguish between $v_\infty = 150$ km s^{-1} and $v_\infty = 1000$ km s^{-1}. We note that if the wind density of Cyg OB2 #12 was a factor of two higher, the blue absorption component would develop up to the corresponding value of v_∞.

Nevertheless, an upper limit on v_∞ may be obtained by means of the Brα/He I 4.048 μm complex. This is apparent in Fig. 9, where we see that ISO observations of this feature clearly resolve both components. Our models indicate that if v_∞ is above ~500 km s^{-1}, both components are blended, while strong emission bluewards of 400 km s^{-1} is present, which is not seen in the data. On their own, these observations lack sufficient S/N and spectral resolution to accurately constrain v_∞, but in conjunction with Hα they jointly provide stronger constraints. Following this approach, we adopt $v_\infty = 400$ km s^{-1} for the remainder of the paper, while recognising that values between 300 and 1000 km s^{-1} cannot *formally* be discarded at present. Regarding this, we suggest that ground based high resolution spectra of Brα and with sufficient S/N to trace the line wings may constitute the best observational constraint available to estimate v_∞.

Likewise, we make use of the shape of Hα and the Brα/He I 4.048 μm complex to estimate β, the parameter characterizing the velocity law. We obtain $\beta = 3$ indicating a relatively flat velocity field. Values of β below 2 or above 4.5 can be ruled out from the line fits.

We are, however, unable to fully reproduce the blue shoulder of the Hα line, noting that this is the case irrespective of the terminal wind velocity adopted in the modeling. In this regard we highlight comparable discrepancies between the synthetic and observed Hα profiles for ζ^1 Sco and HD 190603 (cf. an inability to reproduce the P Cygni absorption features in these stars; Figs. 6 and 7) while in many cases the model fits to BSGs presented by both Crowther et al. (2006) and Searle et al. (2008) also suffer similarly.

Regarding Cyg OB2 #12, the lack of changes in polarisation through the line (Appendix B) strongly argues against any large scale wind asymmetries that might have been supposed to explain this feature. Hence we feel confident in the application of
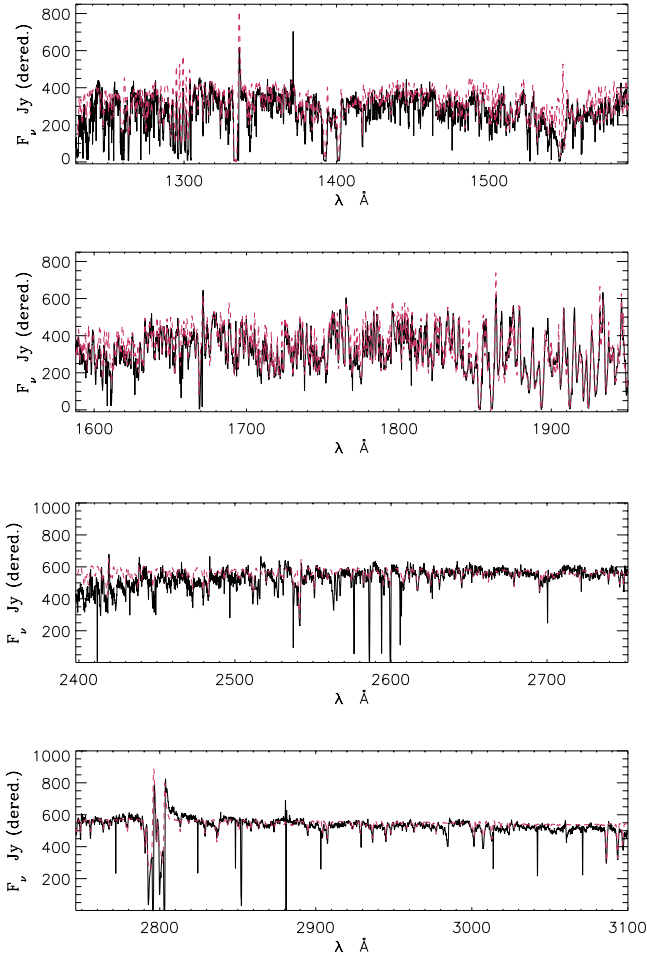
CMFGEN – which adopts spherical symmetry – to this and other stars in this study, while noting that this discrepancy might indicate a shortfall in the physics employed. Subject to this – and the preceding – caveats, we emphasise that the presence of this disagreement between model and observations does not affect our ability to determine the terminal velocity of the wind following the methodology described above[5].

Finally, we were able to derive a mass-loss rate of $\dot{M} = 3.0 \times 10^{-6}\ M_\odot\ \mathrm{yr}^{-1}$ (Table 4). Of course this value is bound to the adopted v_∞ and clumping law. Thus, if v_∞ values of 300, 700 and 1000 km s^{-1} were adopted, fits of similar quality would be obtained for $\dot{M} \sim$ 2.5, 4.0 and $6.5 \times 10^{-6}\ M_\odot\ \mathrm{yr}^{-1}$ respectively.

The main observational constraints which set the run of the clumping law are the H$\alpha - \beta$ and Brα emission components and

---

[5] For completeness we also explored the possibility that the discrepancy between observations and model could be due to the presence of (spatially unresolved) blueshifted nebular emission. Fitting an additional simple Gaussian profile to the blue emission "shoulder" in the Hα and β lines, scaled assuming typical nebular line intensity ratios (Hα/$\beta \sim 2.9$ and Hβ/$\gamma \sim 2.2$), resulted in significantly improved line fits. However, we caution that the adoption of such a solution appears premature at present as no other expected nebular emission lines such as [N II], [S II] or [O I] are present in the spectrum of Cyg OB2 #12; further adaptive optics or coronographic observations to search for compact nebular emission would be of value to determine if such an approach is physically well motivated.

the IR and submillimeter + radio continuum. An onset of the clumping at relatively high velocity ($\sim$200 km s^{-1}) is required to avoid strong emission in the above lines and too great an excess in the IR continuum. On the other hand, we find that a final clumping value of 0.04 is required to reproduce the submillimeter and radio continuum (see Fig. 2).

Our derived mass loss rate presents one of the major differences with respect to previous works. The significantly lower *clumped* mass loss rate of $\dot{M} \sim 3.0 \times 10^{-6}\ M_\odot\ \mathrm{yr}^{-1}$ corresponds to an unclumped ($\dot{M}/f^{0.5}$) rate of $\sim$1.5 $\times 10^{-5}\ M_\odot\ \mathrm{yr}^{-1}$; a factor of $\sim$3 lower than that reported by Leitherer et al. (1982), due to the considerably smaller wind terminal velocity (v_∞) adopted (400 versus 1400 km s^{-1}). The effects of the high degree of wind clumping found for Cyg OB2 #12 mirror recent findings for other massive (evolved) stars (e.g. Najarro et al. 2009; Groh et al. 2009a,b).

Nevertheless, such a *clumping corrected* value is in excess of that found for the less luminous and massive B supergiants studied by Crowther et al. (2006) and Searle et al. (2008). For wind velocities $v_\infty \leq 400$ km s^{-1} the clumping corrected mass loss rate approaches those of known LBVs (Fig. 11; Sect. 5), although the terminal velocity is comparable to BSGs of similar temperature. Adopting $v_\infty \sim 1000$ km s^{-1} leads to a mass loss rate comparable to those of the LBVs, but such a wind velocity is significantly greater than those determined for both LBVs and BSGs of equivalent spectral type. With respect to this, the lack of the low excitation metallic emission lines that characterise cool phase LBV spectra (Sect. 3) is a result of the extremely large radius found for Cyg OB2 #12.

Abundances Fortunately, unlike stars such as HDE 316285 (Hillier et al. 1998), Cyg OB2 #12 does not suffer from a $T_{\rm eff}$/He-abundance degeneracy. Since, as previously described, $T_{\rm eff}$ can be accurately determined from e.g. the Si III/Si II or O II/O I equilibria, we may therefore reasonably constrain the He/H ratio. In Fig. 10 we overplot synthetic spectra constructed with a wide range of He/H abundances on selected He I transitions; note that as expected the best constraints are provided by the weaker, non saturated, transtions. This reveals one of the fundamental results of our study – that Cyg OB2 #12 demonstrates a solar H/He = 10 ratio (by number). Unlike the rest of BHGs analysed in this paper (see Table 4), which clearly demonstrate surface helium enrichment, the He I lines of Cyg OB2 #12 are best reproduced assuming no helium enrichment at all (noting that previous studies of BSGs *adopted* H/He = 5 for all stars considered; Crowther et al. 2006; Searle et al. 2008). Furthermore, even better fits to some of the strong He I lines in the R- (He I 6678 Å), I- (He I 8581 and 8845 Å) and Z-bands (He I 10 830 Å) are obtained if we assume He to be underabundant. Moreover, we find that H/He $\sim$ 8.0 appears to provide a robust lower limit to the abundance ratio, with lower values resulting in unacceptably poor fits to the data (Fig. 10).

We note that given the current stellar temperature and luminosity, the lack of He enrichment at the stellar surfaces is at odds with the predictions from evolutionary models and challenges present theory of stellar evolution of very massive stars. We discuss this somewhat unexpected finding, and the implications for the evolutionary state of Cyg OB2 #12 in Sect. 5. From Table 4 we see indications of CNO processing (N enhancement and CO depletion) in Cyg OB2 #12, though to a lesser extent than for ζ^1 Sco and HD 190603. This result is consistent with the derived H/He ratios.
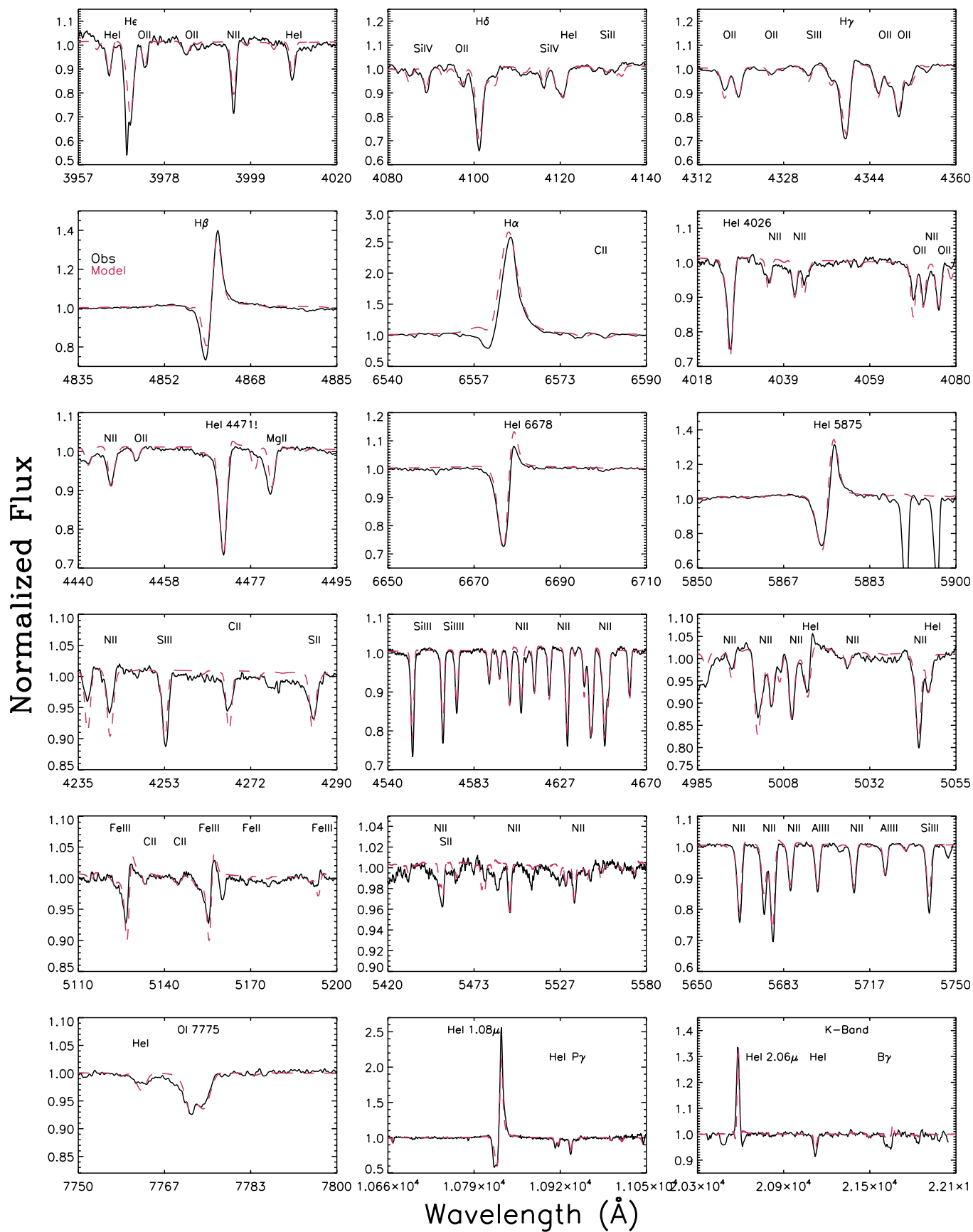
Fig. 6. Comparison of the synthetic spectrum of ζ^1 Sco (red dashed line) with observational data for various transitions between 4090–22 100 Å. Optical data correspond to the 2006 ESO NTT/EMMI run. Note that narrow unlabeled absoption lines are telluric in origin.
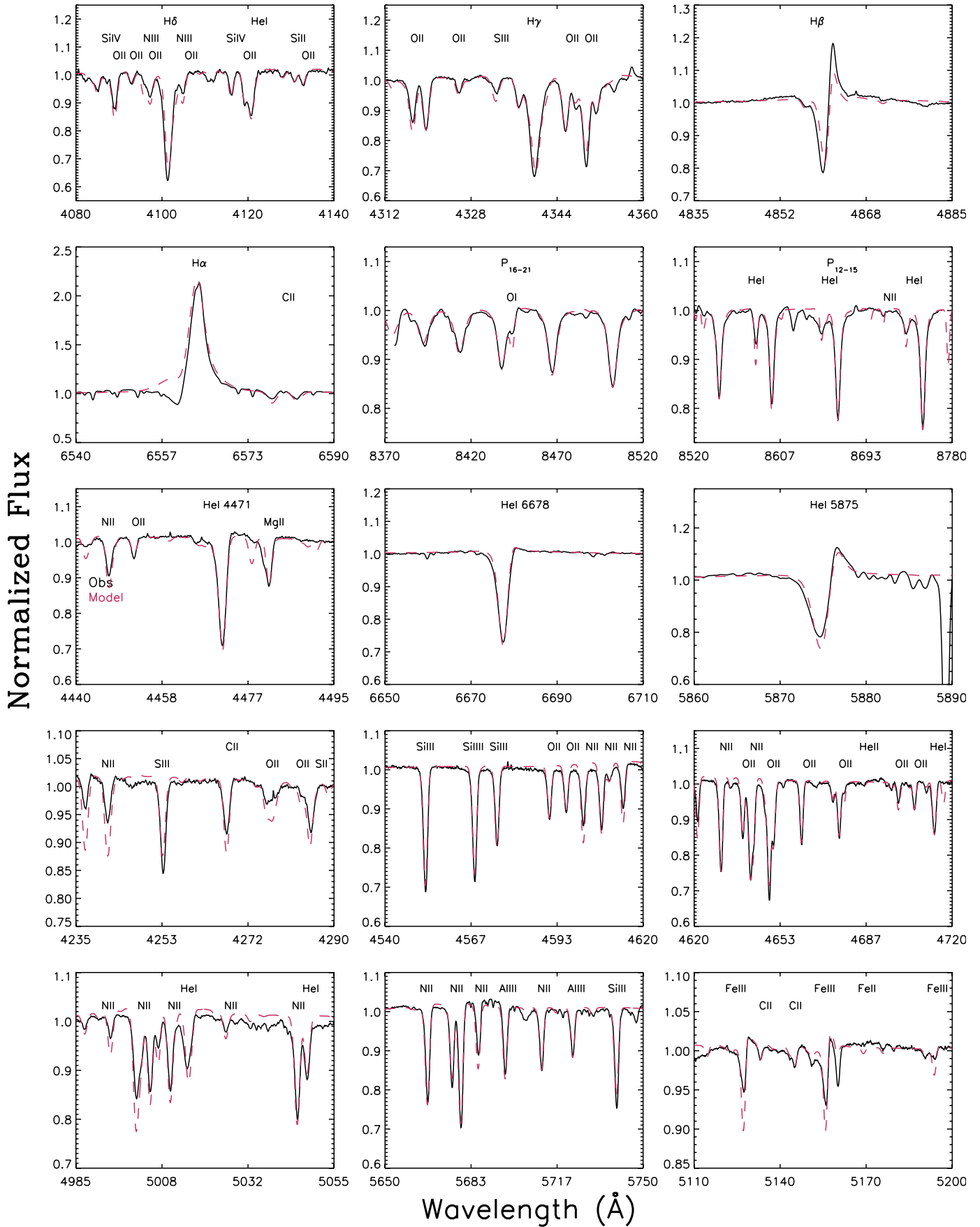
Fig. 7. Comparison of the synthetic spectrum of HD 190603 (red dashed line) to observational data. Optical data correspond to the FEROS data kindly provided by Otmar Stahl. As with ζ^1 Sco (Figs. 7 and C.3), no long-term variability is present between different epochs (not shown). Note that narrow unlabeled absorption lines are telluric in origin.
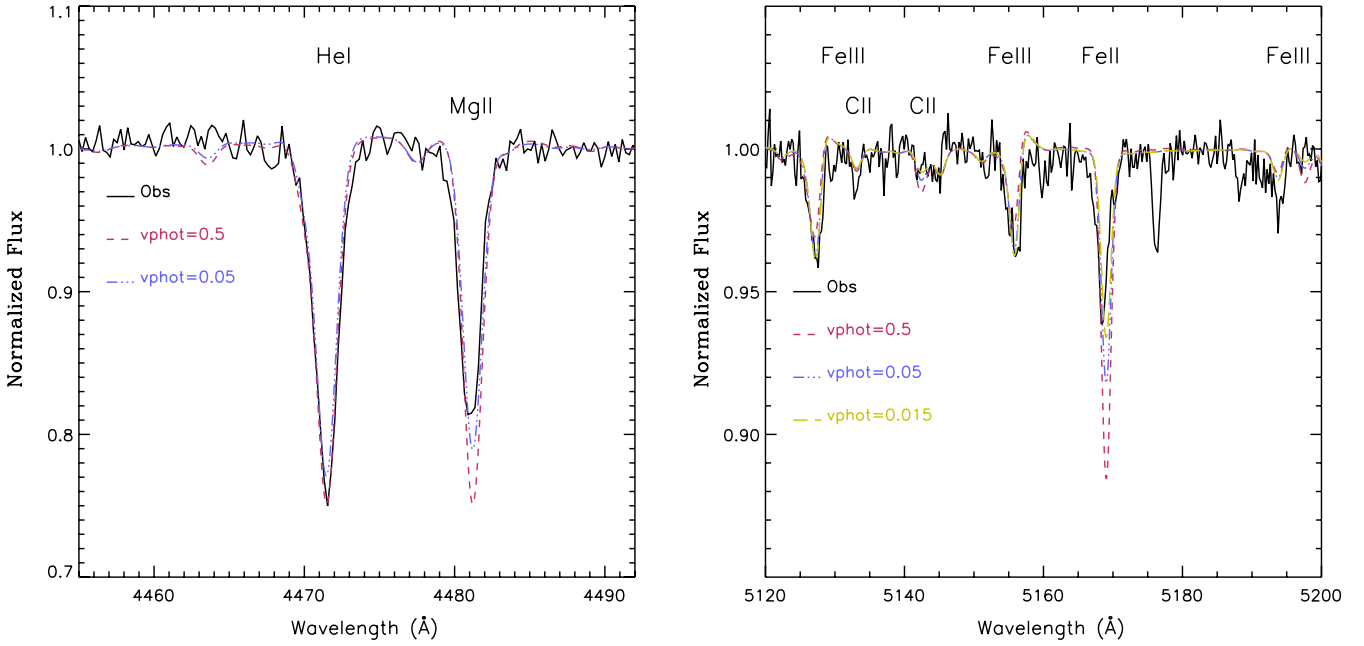
Fig. 8. Importance of the wind/photosphere transition region on the emergent spectrum of Cyg OB2 #12. *Left*: influence of the transition velocity (in units of the sound speed, v_{sound}) on the spectral typing diagnostic lines He I 4471 and Mg II 4481 Å. *Right*: influence on the Fe III/Fe II ionization equilibrium diagnostic lines. The Fe II 5170 Å line is severely affected by the transition velocity while the Fe III lines remain roughly unaltered.
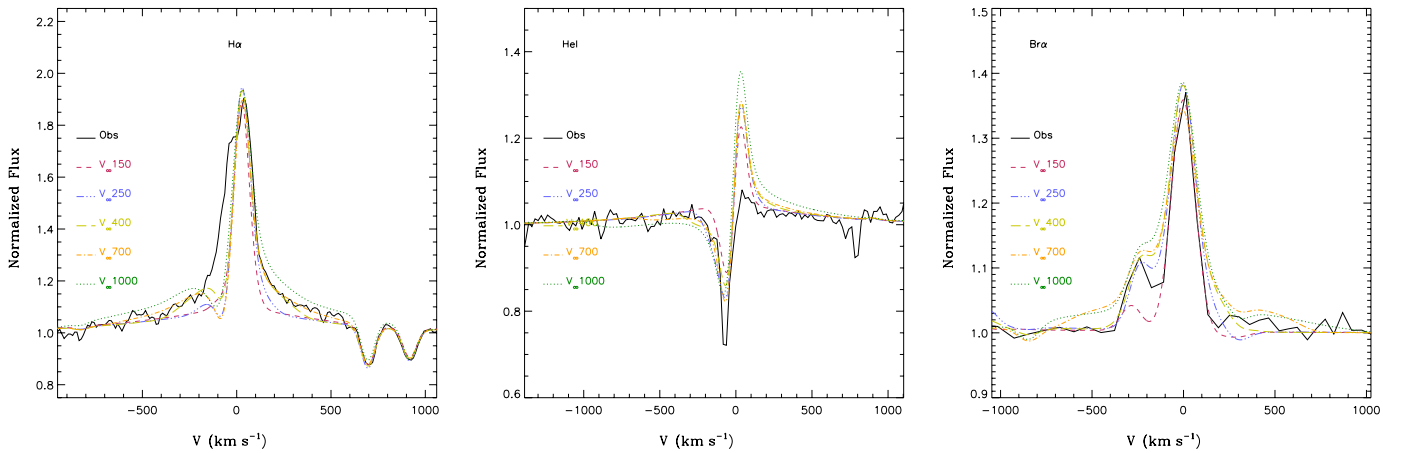

Fig. 9. Estimate of v_∞ for Cyg OB2 #12 from the Hα (*left panel*) and He I 10 830 Å lines (*middle panel*) and Bα/He I 4.048 μm complex (*right panel*).

4.1.1. The unexpected luminosity of Cyg OB2 #12

A critical finding of this analysis is the rather extreme luminosity of Cyg OB2 #12 (e.g. Fig. 12 and Sect. 5); are we overestimating this? An obvious explanation is that a chance alignment with its "host" association leads us to overestimate its distance. If this were the case, the large degree of reddening demonstrated by Cyg OB2 #12 would either be due to a (narrow) sightline of anomalously high interstellar extinction towards *it and only it* – but which nonetheless yielded Diffuse Interstellar Bands (DIBs) comparable to those found for other bona fide association members (e.g. Hanson 2003) – or would be circumstellar in origin (e.g. Massey & Thompson 1991), thus permitting a more normal run of interstellar reddening for a lower distance. However, our model fits to the expanded SED show no evidence for an

IR excess at wavelengths shorter than 30 μm; suggesting that any circumstellar component would have to be significantly cooler than observed around known LBVs, where pronounced emission from warm dust is detected at ≤25 μm (e.g. Egan et al. 2002; Clark et al. 2003a).

A second alternative is that it is a multiple system. Given the recent suggestion of a high binary fraction within Cyg OB2 (Kiminki et al. 2009) and the hard, luminous X-ray emission from Cyg OB2 #12 (Albecete Columbo et al. 2007; Rauw et al. 2005) this would appear to be physically well motivated. To reduce the luminosity of Cyg OB2 #12 such that it was marginally consistent with current theoretical predictions (Sect. 5) would require a companion(s) of equal luminosity. However clear spectroscopic signatures of binarity in terms of (i) radial velocity shifts; (ii) the presence of double lines; and/or (iii) the dilution
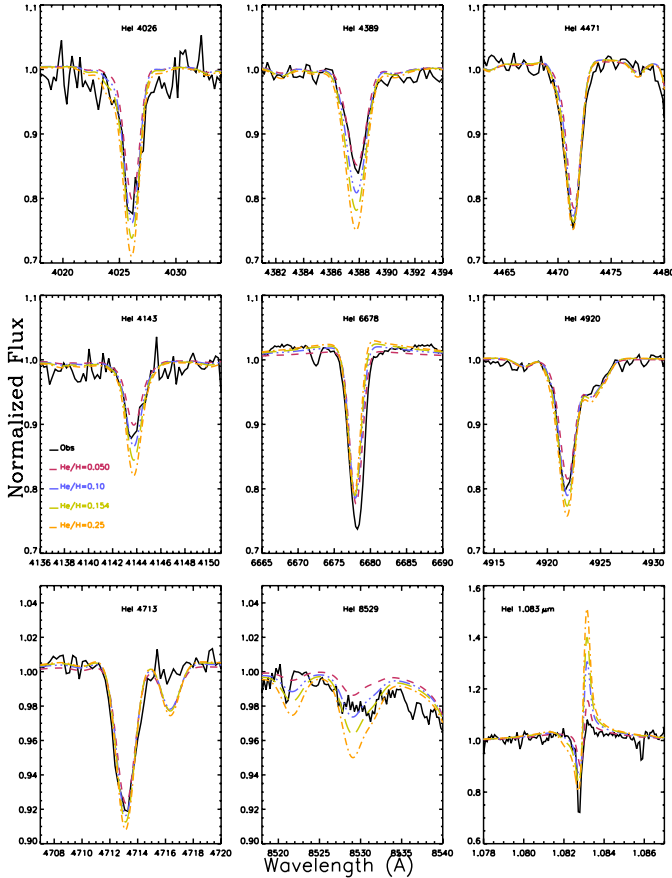
Fig. 10. Montage of selected He I lines in the spectrum of Cyg OB2 #12 with synthetic spectra computed utilising different He/H ratios overplotted.

of spectral features appear absent[6]. Moreover, the excellent model fit to the observed spectral energy distribution also excludes a companion of comparable luminosity but very different temperature.

While not fatal to a binary scenario, these observational constraints would require any putative binary companion of *comparable* luminosity to have an identical spectral type – to avoid its spectral signature being visible – and for the binary to either be very wide or seen face on – to avoid RV shifts in the spectrum. However, the temperature of the hard X-ray component ($kT = 1.8$ keV) implies, via the strong shock condition, that the companion would have to have a wind velocity of ~ 1300 km s^{-1} – inconsistent with the emission arising in the wind collision zone produced by such a "twin" and necessitating the presence of a third, unseen star to yield the high energy emission. While we cannot exclude such a "finely tuned" hierarchical system, we find no compelling evidence for one either.

Lastly, one might suppose that Cyg OB2 #12 were currently undergoing a long-term "LBV eruption" resulting in an increased luminosity. However, while the physical properties of such events are ill constrained we find the current physical properties to be distinct from those of quiescent LBVs (e.g. Sect. 5), while mass loss rates of $\gg 10^{-5}$ $M_\odot$ yr^{-1} are typically inferred for such stars in outburst (Clark et al. 2009). Therefore, while we may not formally exclude any of these possibilities,

---

[6] In particular we note that no (anti-phased) radial velocity shifts indicative of binarity are present in the additional emission components of the Hα, β and γ lines.

we find no compelling observational evidence to support them either and hence consider it likely that the primary BHG within Cyg OB2 #12 is indeed unexpectedly luminous in comparison to theoretical predictions. Moreover, even if its luminosity were reduced via one of these scenarios such that it was consistent with current evolutionary tracks, we note that the revised mass loss rate ($\dot{M} \propto d^{1.5}$) and (unchanged) chemistry would still remain discrepant with respect to field BSGs and BHGs.

4.2. ζ^1 Sco and HD 190603

For the analysis of ζ^1 Sco we adopted a distance $d \sim 1.64$ kpc, based upon the revised estimate for NGC 6231/Sco OB1 (Appendix C); for convenience we also show results for the slightly larger distance of $d \sim 1.9$ kpc adopted in previous works to enable a direct comparison(Crowther et al. 2006). Unfortunately, HD 190603 is not associated with a host cluster making the distance significantly more uncertain. For consistency to prior studies we adopt an identical distance ($d \sim 1.57$ kpc; Crowther et al. 2006), while also presenting results under the assumption that it has an identical intrinsic visual magnitude to ζ^1 Sco.

As in the case of Cyg OB2 #12, several ionization equilibria could be used to determine the stellar temperature. Interestingly we could use three ionization stages of silicon (Si IV/Si III/Si II) for both objects. In the case of HD 190603, our hottest object, the Fe II and N I lines are not detected so we used them in our models as indicators of a lower limit for $T_{\rm eff}$. On the other hand, He II 4686 Å was weakly detected in HD 190603 allowing us to use as well the He II/He I ionization criterium.

Since UV spectra are available for both objects, the terminal velocity, v_∞, could be accurately determined for both objects (e.g. Fig. 5). Given that we are fitting non-simultaneous observations from the UV to the IR we might expect to find some transitions in this wavelength range which are not well fitted by our synthetic spectra. This appears to be the case for C IV 1548–1551 Å, which is significantly underestimated by our models. Moreover these, as well as the Si IV 1394–1403 Å UV lines, are very sensitive to X-rays in this parameter domain; thus they should be regarded with caution.

The main stellar properties of both objects are presented in Table 4. Uncertainties in stellar parameters are similar to those derived for Cyg OB2 #12, except for the effective temperature, which is slightly better constrained $\Delta T_{\rm eff} = \pm 500$ K and the terminal velocity with $\Delta v_\infty = \pm 50$ km s^{-1}. Errors on the H/He ratio are of the order of $\sim 20\%$. Interstellar reddening was also determined; for ζ^1 Sco we found $E(B - V) = 0.66$ and $R_V = 3.3$ and for HD 190603 $E(B - V) = 0.70$ and $R_V = 3.1$.

We found both stars to be less extreme than Cyg OB2 #12 in terms of luminosity, although ζ^1 Sco is still significantly in excess of the range of luminosities spanned by Galactic O9-B5 Ia/b supergiants (Searle et al. 2008; Crowther et al. 2006), even with the downwards revision of the distance. HD 190603 lies in the upper reaches of this distribution, but we caution that this could be subject to revision given the uncertainties in its distance estimate. As expected from their earlier spectral types, they are hotter than Cyg OB2 #12, although the temperatures we find are slightly lower (<1 kK) than previous estimates for these objects. These lower temperature estimates are due in part to the effect of the wind transition region (see Sect. 4.1) and to the use of all available ionization equilibria criteria. Following from these results, spectroscopic mass estimates are significantly lower than that of Cyg OB2 #12 for both stars.
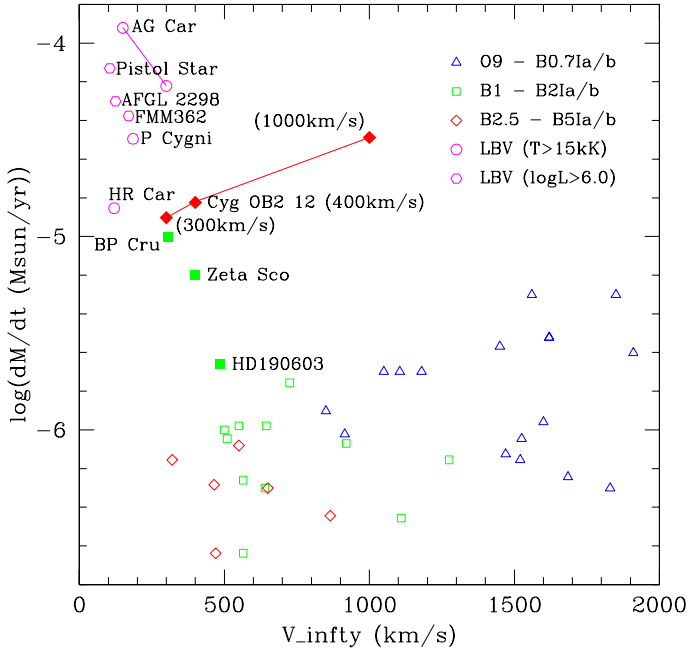
Fig. 11. Comparison of the wind properties of the BHGs to field BSGs (plotted according to spectral type), LBVs of temperature selected to match the BSGs (≥ 15 kK) and those of comparable luminosity to Cyg OB2 #12 ($\log(L/L_\odot) > 6.0$). Data from Crowther et al. (2006), Searle et al. (2008), Najarro et al. (1999, 2009), Clark et al. (2009) and Groh et al. (2009a, 2009b). Inclusion of later BSGs continues the trend to lower mass loss rates and wind velocities (e.g. Markova et al. 2008). Due to the uncertainty in the wind velocity for Cyg OB2 #12, we present 3 pairs of possible values for $v_\infty = 300, 400$ and 1000 km s^{-1} (Sect. 4.1).

Fig. 12. HR diagram with the positions of the BHGs (red diamonds) plotted with respect to the evolutionary tracks of Meynet & Maeder (2005) and the empirical HD limit. The position of HD 80077 *assumes* membership of Pismis 11 and hence a distance of 3.5 kpc (Marco & Negueruela 2009). The positions of other evolved stellar populations are also indicated: black squares – WN7-9h, O4-6 Ia and O4-6 If$^+$ stars within the Arches; purple circles – galactic field BSGs; blue triangles – (candidate) LBVs and WNL stars; green stars – YHGs. Data from Martins et al. (2007, 2008), Crowther et al. (2006), Searle et al. (2008) and Clark et al. (in prep.).

Terminal wind velocities are similar to Cyg OB2 #12, but lie at the lower range of values found for BSGs of comparable spectral type; in contrast the *clumping corrected* mass loss rate for HD 190603 lies at the upper range of those found for B1-2 Ia/b supergiants while that of ζ^1 Sco is considerably in excess of this range (Fig. 11). These compare favourably with previous estimates for these stars (Searle et al. 2008; Crowther et al. 2006; Markova & Puls 2008); although as with Cyg OB2 #12, the high degree of clumping required to fit the spectra provide a significant downwards revision of *absolute* mass loss rates between this and prior studies. Values of $\log g$ are also lower than previous estimates of both stars, due to the greater accuracy afforded us by the inclusion of the higher Balmer and Paschen lines in the spectroscopic datasets.

Finally, in contrast to Cyg OB2 #12, but in line with estimates for field Galactic BSGs, we find a moderate H-depletion (or He-enrichment; H/He ~ 5 by number) for both stars as well as evidence for stronger CNO processing (higher N).

5. Discussion

While the galactic BHG population spans over an order of magnitude in luminosity (Fig. 12), when combined with previous modeling results for BP Cru (Table 4; Kaper et al. 2006), our analyses show the early B1-4 Ia$^+$ hypergiants to be, as expected, rather luminous evolved stars, with HD 80077 and Cyg OB2 #12 appearing to lie above the empirical HD limit (Fig. 12; Marco & Negueruela 2009). In comparison to Galactic BSGs of the same spectral subtypes they are overluminous and
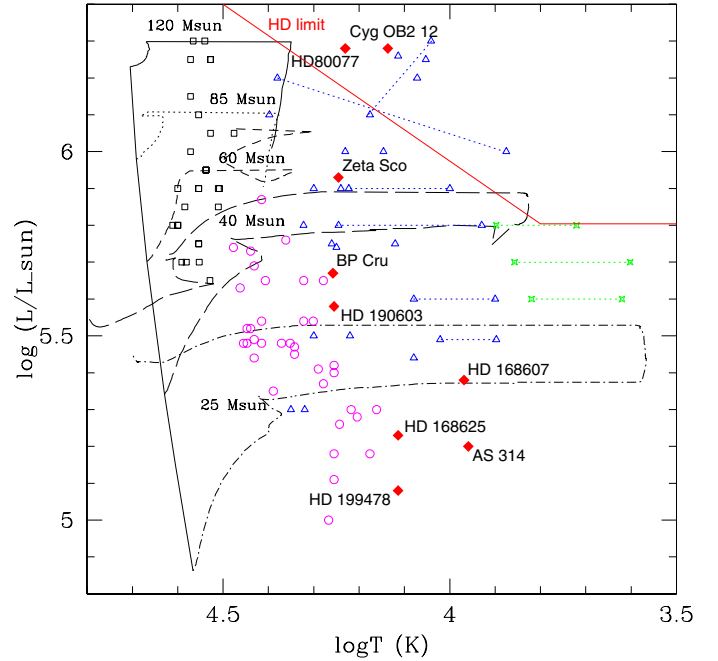
support significantly higher mass loss rates, with wind terminal velocities at the lower end of the range populated by the BSGs.

5.1. The evolutionary status of BHGs

Subject to these observational constraints how may *single* (early) BHGs be understood in evolutionary terms? Several authors have presented evolutionary sequences for massive ($>30\ M_\odot$) stars, including Langer et al. (1994), Crowther et al. (1995), Meynet & Maeder (2005) and Martins et al. (2007, 2008). After the initial O-type main-sequence phase, the recent *empirical* evolutionary scheme of the latter authors may be summarized as:

- $\sim 60-120\ M_\odot$: O Ia $\rightarrow$ OIaf$^+$ $\rightarrow$ WNL + abs $\rightarrow$ WN7
- $\sim 30-60\ M_\odot$: O/B Ia $\rightarrow$ WN9-11h $\rightleftharpoons$ LBV $\rightarrow$ WN8 $\rightarrow$ WN/C.

While not explicit in the above scheme, the properties of LBVs such as AG Car (Groh et al. 2011) and the Pistol star (Najarro et al. 2009) strongly imply that even very massive $M_{\rm ini} > 60\ M_\odot$ stars may experience an LBV phase. Moreover, it is likely that a further subdivision will occur for $M_{\rm ini} < 40\ M_\odot$ to accommodate the high luminosity ($\log(L/L_\odot) \sim 5.8$) cool hypergiants present in clusters such as Westerlund 1 (Wd 1; Clark et al. 2005b):

- $\sim 30-40\ M_\odot$: O $\rightarrow$ OB Ia $\rightarrow$ cool Ia$^+$ $\rightarrow$ WN $\rightarrow$ WC.

Noting that the evolution of spectral classification through the red loop and the final state reached prior to SN is particularly uncertain.

Given that the physical properties of the BHGs appear more extreme than the field BSGs and that they appear co-located with the LBVs on the HR diagram (Fig. 12) a close physical association is suggested and we propose that the early BHGs – *with the notable exception of Cyg OB2 #12* – are the immediate evolutionary progenitors of LBVs for stars of ~40−60 $M_\odot$. Thus, they would form lower mass analogues of the O4-6 Iaf$^+$ stars in the Arches, which Najarro et al. (2004) and Martins et al. (2008) demonstrate are intermediate between the O4-6 Ia and WN7-9ha stars both in terms of the degree of (increasing) chemical evolution and also wind properties, with advancing evolutionary state leading to a reduction in terminal wind velocities coupled with an increase in mass loss rate.

The BHGs appear to follow an analogous evolutionary template, with wind properties approaching those of the LBVs (Fig. 11). Moreover, the BHGs also appear less chemically evolved than (candidate) LBVs[7], again suggesting that they occupy an earlier evolutionary phase. Such an hypothesis appears bolstered by the apparent lack of long-term(secular) variability demonstrated by the early-B HGs (Sect. 3), although we are aware that bona fide LBVs such as P Cygni may also encounter long periods of quiescence.

We emphasise that this evolutionary scheme is appropriate for single stars, but it also appears possible that early-B HGs may form via binary interaction and, through such a channel, potentially from lower mass stars. Wellstein & Langer (1999) present the results of simulations that show the properties of the known binary BP Cru are consistent with quasi-conservative mass transfer in a 26 $M_\odot$ + 25 $M_\odot$ progenitor system. Likewise, the BHG/WNVL transitional object Wd1-13 is the primary of a 23.2 $M_\odot$ + 35.4 $M_\odot$ 9.27 day period binary (Ritchie et al. 2010). This configuration is too compact for the primary to have passed through a BSG phase, and hence presumably formed via an episode of binary mediated mass loss (Sect. A.5), with a likely progenitor mass of ~35 $M_\odot$. In this respect we highlight that Wd1-13 appears spectroscopically distinct from the BHGs considered here, showing pronounced (variable) emission lines in the Paschen series (Fig. A.2 and Ritchie et al. 2010).

Finally, is it possible to place the later (lower luminosity) BHGs into comparable sequences? The consistency of the population of B1-3 Ia and cooler B5-9 Ia$^+$ stars within Wd 1 with theoretical evolutionary isochrones (Negueruela et al. 2010) suggests an extension of the paradigm that BHGs are the more physically extreme direct descendants of hotter O/BSGs to lower progenitor masses (~35 $M_\odot$). However, the placement of these BHGs in a pre- or post-RSG/LBV phase is currently uncertain in the absence of tailored abundance analyses – ESO/VLT observations currently underway will allow this to be directly addressed. Finally, following previous suggestions in the literature (Sect. A.6) – and again in the absence of quantitative analyses – it appears likely that lower luminosity (log($L/L_\odot$) < 5.5) BHGs are post-RSG objects possibly encountering an LBV phase.

5.2. Constraints from the host stellar aggregate

Do other observations support such an evolutionary scheme? Following the above discussion, the stellar populations of both the Arches and Wd 1 are clearly consistent. However we would also predict the presence of early BHGs within the Quintuplet

---

[7] HD 316285 (H/He ∼ 1.5), AG Car (H/He ∼ 2.3), W243 (H/He∼5), P Cygni (H/He ∼ 3.3), FMM362 (H/He ∼ 2.8) and the Pistol Star (H/He ∼ 1.5; Hillier et al. 1998; Groh et al. 2009a; Ritchie et al. 2009; Najarro et al. 2001, 2009, respectively).
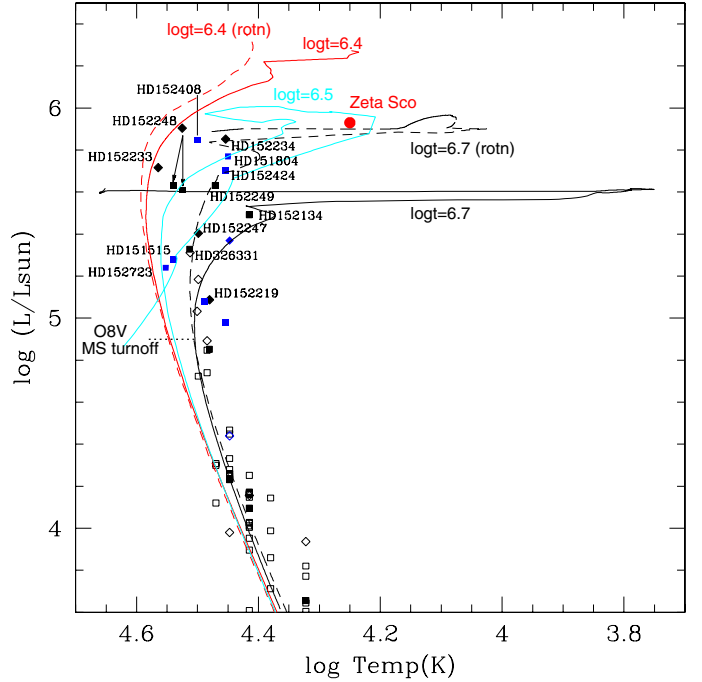

Fig. 13. HR diagram for NGC 6231 (black symbols) and the wider Sco OB1 association (blue symbols) with the non rotating isochrones of Schaller et al. (1992; solid lines) and the rotating isochrones of Meynet & Maeder (2005; dashed line) overplotted. Open and filled symbols represent main sequence and evolved stars, while diamonds indicate binarity. For HD 152248 we plot the position of both the individual components and also that of the integrated system. See Appendix B for details of contruction.

cluster, which is likely to be intermediate in age between these clusters (Figer et al. 1999). While neither these authors nor Liermann et al. (2009) report the presence of BHGs, we note that e.g. LHO96, 100 and 146 – which are classified as O6-8. If by Liermann et al. – have K band spectra identical to that of ζ^1 Sco (Fig. 6). Simply applying the bolometric correction derived from our analysis of ζ^1 Sco yields an estimated log($L/L_\odot$) ∼ 6.0−6.3 for these stars; directly comparable to the Pistol Star and FMM362 (Najarro et al. 2009) and hence consistent with a pre-LBV BHG identification. Further high S/N and resolution observations of these stars would permit quantitative testing of this assertion by virtue of an accurate determination of temperature, luminosity and wind properties.

Encouragingly, stars with a similar K band spectral morphology are also present in the Galactic Centre cluster, where they too are found to be of higher temperature and possess faster, lower mass loss rate winds than the more evolved WNL – and candidate LBV – stars present (Najarro et al. 1997; Martins et al. 2007).

Importantly, are the properties of ζ^1 Sco and Cyg OB2 #12 and their host stellar aggregates consistent with this evolutionary hypothesis? Unfortunately, observations of Cyg OB2 and NGC 6231/Sco OB1 raise the possibility that the stellar populations in both associations are non-coeval (Negueruela et al. 2008; Appendix C). Nevertheless, the physical properties of ζ^1 Sco appear consistent with the population of (initially) rapidly rotating, 5 Myr-old stars present within NGC 6231 (Fig. 13 and Appendix B; noting that the low $v_e \sin i$ of ζ^1 Sco may be understood as a combination of spindown and/or an unfavourable inclination) *or* a somewhat younger (~3.2−4 Myr) population of less rapidly rotating objects that *may* also be
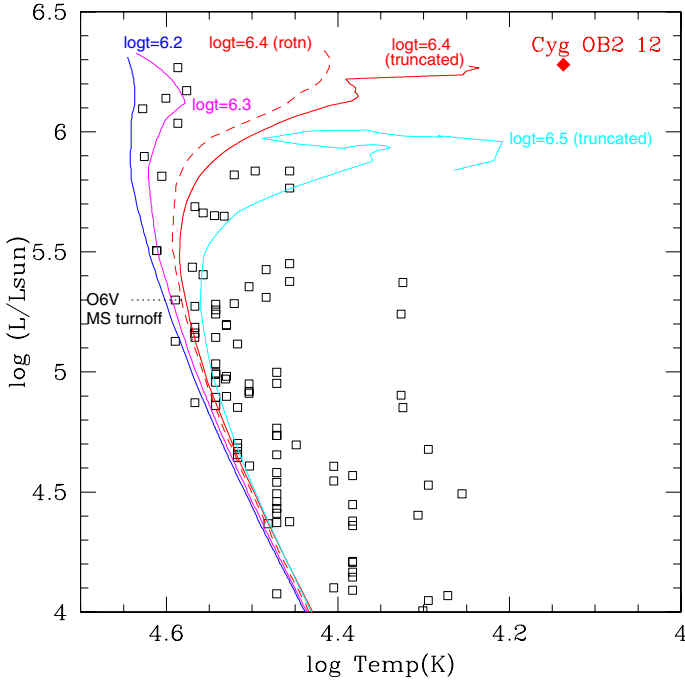
Fig. 14. HR diagram for Cyg OB2 with the non rotating isochrones of Schaller et al. (1992; solid lines) and the rotating isochrone of (Meynet & Maeder 2005; dashed line) overplotted. Data from Negueruela et al. (2008) and Hanson et al. (2003); the reader is refered to these studies for the positions of individual stars, which have been omitted here for reasons of clarity.

present (Appendix B). This would imply a progenitor mass of ~40−60 $M_\odot$ for ζ^1 Sco, depending on age and initial rotation, broadly consistent with the current spectroscopic mass of ~36 $M_\odot$.

Finally, we address Cyg OB2 #12. As highlighted previously, this star appears difficult to accomodate in the current evolutionary scheme due to the combination of high luminosity and low temperature displacing it from any theoretical isochrones applicable to Cyg OB2 (Fig. 14; Negueruela et al. 2008). While its co-location in the HR diagram with *bona fide* LBVs such as the Pistol Star, FMM 362 and AFGL 2298 (Fig. 12) suggests a similar nature, the long-term stability combined with its relatively unevolved chemsitry – and critically solar H/He ratio – appear to exclude such an identification. We are thus currently unable to place Cyg OB2 #12 into a coherent evolutionary scheme, noting that with a *current* spectroscopic mass of ~110 $M_\odot$ – significantly in excess of both the Pistol Star and FMM 362 (Najarro et al. 2009) – one might expect it to evolve through a much hotter O4-6I/Iaf$^+$/WNLha evolutionary sequence.

In this respect, the results of a quantative analysis of HD 80077 would be of particular interest, given its apparent similarly extreme luminosity (Marco & Negueruela 2009). Such an analysis has been performed for the M 33 B1 Ia$^+$ star [HS80] 110A by Urbaneja et al. (2005) which yielded stellar parameters that, like Cyg OB2 #12, both place it above the HD-limit and appear to distinguish it from known LBVs[8]. This finding appears to suggest that there might indeed be an hitherto unidentified (but rarely traversed?) evolutionary pathway that leads to the production of very luminous but comparatively cool BHGs at very high stellar masses.

---

[8] $\log(L/L_\odot) \sim 6.5$, $T_{\rm eff} \sim 21$ kK, $v_\infty \sim 750$ km s^{-1} and $\dot{M} = 1.06 \times 10^{-5}$ $M_\odot$ yr^{-1}.

6. Conclusions

In order to determine the physical properties and hence evolutionary state of Galactic early-B hypergiants, we have undertaken new quantitative analyses of Cyg OB2 #12, ζ^1 Sco and HD 190603 and employ previous model results for BP Cru. Synthetic spectra and SEDs were calculated and compared to comprehensive UV/optical–radio spectroscopic and photometric datasets compiled from the literature and supplemented by new and previously unpublished observations. Building on this effort, we also constructed exhaustive spectroscopic and photometric histories for all Galactic BHGs in order to test the assertion that they are physical identifiable with LBVs.

Turning first to stellar variability and both the early- and late-B HGs demonstrated the rapid (~days) spectroscopic and photometric variability that is symptomatic of the aspherical wind substructure and photospheric pulsations that characterises luminous early stars. While low-luminosity, late-B HGs have long be known to undergo LBV excursions (e.g. HD 160529) we found no evidence for such secular variability amongst the early, high luminosity BHGs, with the possible exception of ζ^1 Sco in the sparse photometric data obtained prior to the 20th Century. In this regard it is interesting that both Cyg OB2 #12 and HD 80077 appear to lie above the empirical HD limit.

Model results reveal that the early-B HGs have physical properties – luminosity, wind terminal velocity, mass loss rate and chemical abundances – intermediate between Galactic BSGs and LBVs of comparable temperature, suggesting they provide a link between both evolutionary phases for stars of inital mass between ~40−60 $M_\odot$. In this respect, they would play a similar role to the more massive and luminous O4-6Iaf$^+$ objects for stars in the ~60−120 $M_\odot$ range (Najarro et al. 2004; Martins et al. 2008). The simultaneous presence of populations of early B1-3 Ia supergiants and mid-late B5-9 Ia$^+$ BHGs within Wd 1 suggest that BHGs are potentially the immediate descendents of stars with initial masses as low as 30−35 $M_\odot$. However, the presence of early-B HGs within this cluster indicates that a parallel channel may also lead to this phase via close binary evolution.

Nevertheless, Wd 1 and the Quintuplet provide direct observational tests of the evolutionary sequence proposed; in the former cluster the BHGs should be more chemically evolved than the BSG population but less than the RSGs that are present, while in the latter cluster one would expect to find a population of early BHGs; observations aimed at verifying both hypotheses will be undertaken later this year.

The apparent physical association of ζ^1 Sco with NGC 6231/Sco OB1 also allows us to test this scenario. Encouragingly, we find that the physical properties derived from our analysis are consistent with the observed stellar population of this region and in turn with theoretical isochrones for stars of between 3.2–5 Myr age – further discrimination is difficult in the absence of an absolute rather than projected rotational velocity.

Conversely, the combination of extreme luminosity and cool temperature of Cyg OB2 #12 is inconsistent with theoretical isochrones, *assuming membership of Cyg OB2*. Given its co-location with a handful of bona fide LBVs above the HD limit it might be supposed to be a similar object, but a combination of (i) a lack of the characteristic LBV variability; (ii) extreme *current* stellar mass; and (iii) lack of chemical evolution differentiate it from these. We are therefore currently unable to place this star in a consistent evolutionary scheme, noting that Negueruela et al. (2008) also find that a number of the hottest and most luminous stars within Cyg OB2 are difficult to accommodate in

a formation scenario for the association where the most recent epoch of star formation occurred ~2.5 Myr ago.

Nevertheless, we note that the stability of Cyg OB2 #12 for the last century would appear to indicate that the HD limit does not appear to define a region of the HR diagram utterly inimical to the presence of massive stars, but a combination of (pulsational?) instabilities and extreme mass loss rates presumably prevent stars residing above it for large fractions of their lifetime. Indeed, from Fig. 12 we may see that in addition to highly luminous BHGs such as Cyg OB2 #12 the *empirical* HD limit appears to be delineated by LBVs and other closely related (variable) stars such as the cool hypergiants and the WNVLs, further suggesting that it should not be regarded as a firm barrier to stellar stability, nor the location at which the onset of instabilities occurs. In this regard the B1 Ia$^+$ star [HS80] 110A and the cool F-hypergiant B324 (both located in M 33) are of considerable interest; like Cyg OB2#12, the combination of temperatures and luminosities they demonstrate are not replicated by current evolutionary tracks and place both stars well above the HD limit (Urbaneja et al. 2005; Clark et al. 2012). Quantitative modeling of the Galactic BHG HD 80077 would therefore be of considerable interest to see whether this too violated the HD limit.

Moreover, despite residing above the HD limit, we find an Eddington parameter, Γ_{Edd}, of only ~0.41 (and $\Gamma_{Total} \sim 0.56$ at $R(\tau_{Ross} = 2/3)$ for Cyg OB2 #12); below the Eddington limit. Unfortunately, in the absence of an inclination we may not determine how close Cyg OB2 #12 is to the rotationally modified Eddington limit, although we note that the Eddington parameter for it is lower than Groh et al. (2011) found for AG Car at any epoch. Given that AG Car is also a known rapid rotator but has not been observed at, or to have exceeded, the rotationally modified Eddington limit we suspect the same to be true for Cyg OB2 #12. From this we might therefore conclude that the HD-limit is not the direct result of a star (b)reaching the rotationally modified Eddington limit. Indeed, Groh et al. (2011) show that AG Car most closely approaches the rotationally modified Eddington limit during its hot, compact phases when, in contrast to its cool extended state, it lies *beneath* the HD limit (Fig. 12).

References

Abbott, D. C., Bieging, J. H., & Churchwell, E. 1981, ApJ, 250, 645
Abbott, D. C., Telesco, C. M., & Wolff, S. C. 1984, ApJ, 279, 225
Adelman, S. J., & Albayrak, B. 1997, IBVS, 4541, 1
Adelman, S. J., Yuce, K., & Engin, S. 2000, IBVS, 4946, 1
Ahmad, I. I. 1952, ApJ, 115, 341
Albacete Columbo, J. F., Flaccomio, E., Micela, G., Sciortino, S., & Damiani. F. 2007, A&A, 464, 211
Allen, D. A. 1973, MNRAS, 161, 145
Anders, E., & Grevesse, N. 1989, GeCoA, 53, 197
Andrews, P. H. 1968, MmRAS, 72, 35
Andrillat, Y., Jaschek, C., & Jaschek, M. 1995, A&AS, 112, 475
Ankay, A., Kaper, L., de Bruijne, J. H. J., et al. 2001, A&A, 370, 170
Asplund, M., Grevesse, N., & Jacques Sauval, A. 2006, NuPhA, 777, 1
Baume, G., Vázquez, R. A., & Feinstein, A. 1999, A&AS, 137, 233
Barsukova, E. A., Lebedeva, I. A., Chargejshvili, K. B., & Chentsove, E. L. 1982, AISAO, 16, 34
Beals, C. S. 1946, JRASC, 40, 156
Becker, R. H., & White, R. L. 1985, ASSL, 116, 139
Benaglia, P., Vink, J. S., Martí, J., et al. A&A, 2007, 467, 1265
Bidelman, W. P. 1954, PASP, 66, 249
Bieging, J. H., Abbott, D. C., & Churchwell, E. B. 1989, ApJ, 340, 518
Bisiacchi, G. F., Firmani, C., Ortega, R., & Peniche, R. 1976, Rev. Mex. Astron. Astrofis., 2, 13
Blanco, V. M., Demers, S., Douglass, G. G., & FitzGerald, M. P. 1968, Publ. US Naval Obs. 21
Blum, R. D., Ramond, T. M., Conti, P. S., Figer, D. F., & Sellgren, K. 1997, AJ, 113, 1855
Bohannan, B., & Crowther, P. A. 1999, ApJ, 511, 374
Bord, D. J. 1979, A&A, 77, 309
Botto, P., & Hack, M. 1962, MmSAI, 33, 159
Bouigue, R., Boulon, J., & Pedoussaut, A. 1961, Ann. Observ. Astr. Meteo. Toulouse, 28, 33
Bromage, G. E. 1971, Nature, 230, 172
Burnichon, M. L., & Garnier, R. 1976, A&AS, 24, 89
Burki, G. 1978, A&A, 65, 357
Burki, G., Heck, A., Cassatella, A., & Binchi, L. 1982, A&A, 107, 205
Buscombe, W. 1962, MNRAS, 124, 189
Buscombe, W., & Kennedy, P. M. 1968, MNRAS, 139, 341
Buscombe, W., & Kennedy, P. M. 1969, MNRAS, 143, 1
Cannon, A. J. 1901, Harvard Obs. Ann., 28, part 2, 177, note 43
Chaldu, R., Honeycutt, R. K., & Penston, M. V. 1973, PASP, 85, 87
Chentsov, E. L. 1955, Ap&SS, 232, 217
Chentsov, E. L., Ermakov, S. V., Klochkova, V. G., et al. 2003, A&A, 397, 1035
Clark, J. S., Egan, M. P., Crowther, P. A., et al. 2003, A&A, 412, 185
Clark, J. S., Larionov, V. M., & Arkharov, A. 2005a, 435, 239
Clark, J. S., Negueruela, I., Crowther, P. A., & Goodwin, S. P. 2005b, A&A, 434, 949
Clark, J. S., Muno, M. P., Negueruela, I., et al. 2008, A&A, 477, 147
Clark, J. S., Crowther, P. A., Larionov, V. M., et al. 2009, A&A, 507, 1555
Clark, J. S., Ritchie, B. W., & Negueruela, I. 2010, A&A, 514, 87
Clark, J. S., Arkharov, A., Larionov, V., et al. 2011, BSRSL, 80, 361
Clark, J. S., Castro, N., Garcia, M., et al. 2012, A&A, 541, A146
Clarke, A. J., Oudmaijer, R. D., & Lumsden, S. L. 2005, MNRAS, 363, 1111
Code, A. D., & Houck, T. E. 1958, PASP, 70, 261
Comerón, F., Pasquali, A., Rodighiero, G., et al. 2002, A&A, 389, 874
Conti, P. S., & Howarth, I. D. 1999, MNRAS, 302, 145
Contreras, M. E., Rodriguez, L. F., Gomez, Y., & Velazquez, A. 1996, ApJ, 469, 329
Contreras, M. E., Montes, G., & Wilkin, F. P. 2004, Rev. Mex. Astron. Astrofis., 40, 53
Cousins, A. W. J. 1952, MNSSA, 11, 9
Crawford, D. L., Barnes, J. V., & Golson, J. C. 1971, AJ, 76, 1058
Crowther, P. A., & Evans, C. J. 2009, A&A, 503, 985
Crowther, P. A., Smith, L. J., Hillier, D. J., & Schmutz, W. 1995, A&A, 293, 427
Crowther, P. A., Lennon, D. J., & Walborn, N. R. 2006, A&A, 446, 279
Dachs, J., Maitzen, H.-M., Moffat, A. F. J., Sherwood, W. A., & Stift, M. 1977, A&A, 56, 417
Davies, B., Oudmaijer, R. D., & Vink, J. S. 2005, A&A, 439, 1107
Dessart, L., & Hillier, D. J. 2010, MNRAS, 405, 2141
Drout, M. R., Massey, P., Meynet, G., Tokarz, S., & Caldwell, N. 2009, ApJ, 703, 441
Egan, M. P., Price, S. D., & Gugliotti, G. M. 2001, BAAS, 34 561
Egan, M. P., Clark, J. S., Mizuno, D. R., et al. 2002, ApJ, 572, 288
ESA, The Hipparcos and Tycho Catalogues, 1997, ESA SP, 1200
Evans, D. S., Menzies, A., & Stoy, R. H. 1959, MNRAS, 119, 638
Fraser, M., Dufton, P. L., Hunter, I., & Ryans, R. S. I. 2010, MNRAS, 404, 1306
Feinstein, A. 1968, ZA, 68, 29
Feinstein, A., & Marraco, H. G. 1979, AJ, 84, 1713
Fernie, J. D. 1983, ApJS, 52, 7
Figer, D. F., McLean, I. S., & Morris, M. 1999, ApJ, 514, 202
Frew, D. J. 2004, J. Astron. Data, 10, 6
van Genderen, A. M. 2001, A&A, 366, 508
van Genderen, A. M., van Leeuwen, F., & Brand, J. 1982, A&AS, 47, 591
Golay, M. 1958, Publ. Obs. Geneve Ser. A, 57, 373
González, R. F., & Cantó, J. 2008, A&A, 477, 373
Gottlieb, E. W., & Liller, W. 1978, ApJ, 225, 488
Groh, J. H., Damineli, A., & Jablonski, F. 2007, A&A, 465, 993
Groh, J. H., Hillier, D. J., & Damineli, A. 2009a, ApJ, 698, 1698
Groh, J. H., Hillier, D. J., Damineli, A., et al. 2009b, ApJ, 705, L25
Groh, J. H., Hillier, D. J., & Damineli, A. 2011, ApJ, 736, 46
Gvaramadze, V. V., Kniazev, A. Y., & Fabrika, S. 2010, MNRAS, 405, 1047
Hammerschlag-Hensberge, G., Zuiderwijk, W. J., van den Heuvel, E. P. J., & Hensberge, H. 1976, A&A, 49, 321
Hammerschlag-Hensberge, G., Zuiderwijk, W. J., De Loore, C., & van den Heuvel, E. P. J. 1979, A&A, 76, 245
Hanson, M. M. 2003, ApJ, 597, 957
Hanson, M. M., Conti, P. S., & Rieke, M. J. 1996, ApJS, 107, 281
Hanson, M. M., Rieke, G. H., & Luhman K. L. 1998, AJ, 116, 1915

Hanson, M. M., Kudritzki, R.-P., Kenworthy, M. A., Puls, J., & Tokunaga, A. T. 2005, ApJS, 161, 154
Harries, T. J., & Howarth, I. D. 1996, A&AS, 119, 61
Harris, D. H., Woolf, N. J., & Rieke, G. H. 1978, ApJ, 226, 829
Harries, T. J., Howarth, I. D., & Evans, C. J. 2002, MNRAS, 337, 341
Heger, A., Langer, N., & Woosley, S. E. 2000, ApJ, 528, 368
Hendry, M. A., Smartt, S. J., Skillman, E. D., et al. 2008, MNRAS, 388, 1127
Hill, G. M., Moffat, A. F. J., St-Louis, N., & Bartzakos, P. 2000, MNRAS, 318, 402
Hillier, D. J., & Miller, D. L. 1998, ApJ, 496, 407
Hillier, D. J., & Miller, D. L. 1999, ApJ, 519, 354
Hillier, D. J., Crowther, P. A., Najarro, F., & Fullerton, A. W. 1998, A&A, 340, 483
Hiltner, W. A. 1956, ApJS, 2, 389
Hoffleit, D. 1933, Harvard Obs. Bull., 892, 19
Hubeny, I., & Lanz, T. 1995, ApJ, 439, 875
Houck, J. R., Roellig, T. L., van Cleve, J., et al. 2004, ApJS, 154, 18
Humphreys, R., & Davidson, K. 1979, ApJ, 232, 409
Humphreys, R., & Davidson, K. 1994, PASP,106, 1025
Humphreys, R., Davidson, K., & Smith, N. 1999, PASP, 111, 1124
Hutchings, J. B. 1968, MNRAS, 141, 219
Hutchings, J. B. 1970, MNRAS, 147, 161
Hutchings, J. B. 1976, PDAO, 14, 355
Hutchings, J. B. 1981, PASP, 93, 50
Jaschek, M., & Jaschek, C. 1973, PASP, 85, 127
Jaschek, C., Jaschek, M., & Kucewicz, B. 1964, ZA, 59, 108
Johnson, H. L. 1965, ApJ, 141, 923
Johnson, H. L., & Borgman, J. 1963, BAN, 17, 115
Johnson, H. L., & Morgan, W. W. 1953, ApJ, 117, 313
Johnson, H. L., Iriarte, B., Mitchell, R. I., & Wisniewski, W. Z. 1966, Comm. Lunr Pan. Lab., 4, 99
Johnson, H. L. 1968, in Stars and Stellar Systems VII, ed. B. M. Middlehurst, & L. A. Aller (Chicago: Univ. of Chicago Press), 167
Kaper, L., Lamers, H. J. G. L. M., Ruymaekers, E., van den Heuvel, E. P. J., & Zuidervijk, E. J. 1995, A&A, 300, 446
Kaper, L., van der Meer, A., & Najarro, F. 2006, A&A, 457, 595
Kastner, J. H., Buchanan, C. L., Sargent, B., & Forrest W. J. 2006, ApJ, 638, L29
Kaufer, A., Stahl, O., Wolf, B., et al. 1996, A&A, 305, 887
Kaufer A., Stahl, O., Wolf, B., et al. 1997, A&A, 320, 273
Kaufer, A., Stahl, O., Prinja, R. K., & Witherick, D. 2006, A&A, 447, 325
Keenan, P. C. 1971, Contr. KPNO No. 554, 35
Kilkenny, D., can Wyk, F., Marang, F., et al. 1993, SAAOC, 15, 73
Kiminki, D. C., Kobulnicky, H. A., Kinemuchi, K., et al. 2007, ApJ, 664, 1102
Kiminki, D. C., Kobulnicky, H. A., Gilbert, I., Bird, S., & Chunev, G. 2009, AJ, 137, 4608
Klochkova, V. G., & Chentsov, E. L. 2004, Astron. Rep., 48, 1005
Knödlseder, J. 2000, A&A, 360, 539
Knoechel G., & Moffat, A. F. J. 1982, A&A, 110, 263
Kobulnicky, H. A., Molnar, L. A., & Jones, T. J. 1994, AJ, 107, 1433
Koen, C., & Eyer, L. 2002, MNRAS, 331, 45
Kruszewski, A. 1971, AJ, 76, 576
Kudritzki, R.-P. 2010, AN, 331, 459
Langer, N., Hamann, W.-R., Lennon, M., et al. 1994, A&A, 290, 819
van Leeuwen, F., Evans, D. W., Grenon, M., et al. 1997, A&A, 323, L61
van Leeuwen, F., van Genderen, A. M., & Zegelaar, I. 1998, A&AS, 128, 117
Lefèvre, L., Marchenko, S. V., Moffat, A. F. J., & Acker, A. 2009, A&A, 507, 1141
Leitherer, C., & Robert, C. 1991, ApJ, 377, 629
Leitherer, C., & Wolf, B. 1984, A&A, 132, 151
Leitherer, C., Hefele, H., Stahl, O., & Wolf, B. 1982, A&A, 108, 102
Leitherer, C., Stahl, O., Wolf, B., & Bertout, C. 1984, A&A, 140, 199
Lennon, D. J., Dufton, P. L., & Fitzsimmons, A. 1992, A&AS, 94, 569
Lenorzer, A., Vandenbussche, B., Morris, P., et al. 2002, A&A, 384, 473
Lesh, J. R. 1968, ApJS, 17, 371
Liermann, A., Hamann, W.-R., & Oskinova, L. M. 2009, A&A, 494, 1166
Lopez, J. A., & Walsh, J. R. 1984, Rev. Mex. Astron. Astrofis., 9, 3
Marco, A., & Negueruela, I. 2009, A&A, 493, 79
Markova, N., & Puls, J. 2008, A&A, 478, 823
Markova, N., & Valchev, T. 2000, A&A, 363, 995
Martins, F., & Plez, B. 2006, A&A, 457, 637
Martins, F., Schaerer, D., & Hillier, D. J. 2005, A&A, 436, 1049
Martins, F., Genzel, R., & Hillier, D. J. 2007, A&A, 468, 233
Martins, F., Hillier, D. J., Paumard, T., et al. 2008, A&A, 478, 219
Massey, P., & Thompson, A. B. 1991, AJ, 101, 1408
Mathewson, D. S., & Ford, V. L. 1970, MemRAS, 74, 139
McLean, I. S. 1979, MNRAS, 186, 265
McLean, I. S., & Clarke, D. 1979, MNRAS, 186, 245
McMillan, R. S., & Tapia, S. 1977, ApJ, 212, 714

Merrill, P. W., & Burwell, C. G. 1933, ApJ, 78, 87
Merrill, P. W., & Burwell, C. G. 1943, ApJ, 98, 162
Merrill, P. W., Humason, M. L., & Burwell, C. G. 1925, ApJ, 61, 389
Meynet, G., & Maeder, A. 2005, A&A, 429, 581
Miroshnichenko, A. S., Chentsov, E. L., & Klochkova, V. G. 2000, A&AS, 144, 379
Moffat, A. F. J., & Fitzgerald, P. M. 1977, A&A, 54, 263
Moffett, T. J., & Barnes III, T. G. 1979, PASP, 91, 180
Moon, D.-S., Kaplan, D. L., Reach, W. T., et al. 2007, ApJ, 671, L53
Morel, T., Marchenko, S. V., Pati, A. K., et al. 2004, MNRAS, 351, 552
Morgan, W. W., Johnson, H. L., & Roman, N. G. 1954, PASP, 66, 85
Morgan W. W., Code, A. D., & Whitford, A. E. 1955, ApJS, 2, 41
Munari, U., Siviero, A., Bienaymé, O., et al. 2009, A&A, 503, 511
Najarro, F. 2001, P Cygni 2000: 400 Years of Progress, ed. M. de Groot, & C. Sterken (San Francisco, CA: ASP), ASP Conf. Ser., 233, 133
Najarro, F., Krabbe, A., Genzel, R., et al. 1997, A&A, 325, 700
Najarro, F., Hillier, D. J., Figer, D., & Geballe, T. R. 1999, in The Central Parsecs of the Galaxy, ed. H. Falcke et al. (San Francisco, CA: ASP), ASP Conf. Ser., 186, 340
Najarro, F., Figer, D. F., Hillier, D. J., & Kudritzki, R. P. 2004, ApJ, 611, L105
Najarro, F., Figer, D. F., Hillier, D. J., Geballe, T. R., & Kudritzki, R. P. 2009, ApJ, 691, 1816
Negueruela, I., Marco, A., Herrero, A., & Clark, J. S. 2008, A&A, 487, 575
Negueruela, I., Clark, J. S., & Ritchie, B. W. 2010, A&A, 516, 78
Nicolet, B. 1978, A&AS, 34, 1
Nordsieck, K. H., Wisniewski, J., Babler, B. L., et al. 2001, 400 Years of Progress, ed. M. de Groot, & C. Sterken (San Francisco, CA: ASP), ASP Conf. Ser., 233, 261
Nordstrom, B. 1975, A&AS, 21, 193
Parkes, G. E., Culhane, J. L., Mason, K. O., & Murdin, P. G. 1980, MNRAS, 191, 547
Payne-Gaposchkin, C., & Gaposchkin, S. 1938, Variable Stars (Cambridge, Mass.: Harvard College Observatory), 329
Percy, J. R., & Welch, D. L. 1983, PASP, 95, 491
Percy, J. R., Palaniappan, R., Seneviratne, R., Adelman, S. J., & Markova, N. 2008, PASP, 120, 311
Perry, C. L., Hill, G., & Christodoulou, D. M. 1991, A&AS, 90, 195
Perryman, M. A. C., Lindegren, L., & Kovalevsky, J., et al. 1997, A&A, 323, L49
Persi, P., & Ferrari-Toniolo, M. 1982, A&A, 112, 292
Petrovic, J., Langer, N., & van der Hucht, K. A. 2005, A&A, 435, 1013
Pickering, E. C., & Fleming, W. P. 1896, ApJ, 4, 369
Rabod, D., Cramer, N., & Bernasconi, P. A. 1997, A&A, 325, 167
Rauw, G., De Becker, M., & Linder, N. 2005, in Proc. Massive Stars and High-Energy Emission in OB Associations, a workshop of the JENAM 2005 Distant Worlds, held in Liège, Belgium, ed. G. Rauw, Y. Nazé, R. Blomme, & E. Gosset (Liège), 103
Reed, B. C. 2003, AJ, 125, 2513
Reipurt, B. 2008, Handbook of star forming regions, Volume II: The southern sky ASP Monograph Publications, ed. B. Reipurth (San Francisco, CA: ASP), 5, 401
Rimmer, W. B. 1930, MmMtS, 2, 1
Ritchie, B. W., Clark, J. S., Negueruela, I., & Najarro, F. 2009, A&A, 507, 1597
Ritchie, B. W., Clark, J. S., Negueruela, I., & Langer, N. 2010, A&A, 520, A48
Rivinius, T., Stahl, O., Wolf, B., et al. 1997, A&A, 318, 819
Robberto, M., & Herbst, T. M. 1998, ApJ, 498, 400
Rosendhal, J. D. 1973, ApJ, 186, 909
Sana, H., Rauw, G., & Gosset, E. 2001, A&A, 370, 121
Sana, H., Gosset, E., Rauw, G., Sung, H., & Vreux, J.-M. 2006a, A&A, 454, 1047
Sana, H., Rauw, G., Nazeé, Y., Gosset, E., & Vreux, J.-M. 2006b, MNRAS, 372, 661
Sana, H., Rauw, G., Sung, H., Gosset, E., & Vreux, J.-M. 2007, MNRAS, 377, 945
Sana, H., Gosset, E., Nazé, Y., Rauw, G., & Linder, N. 2008, MNRAS, 386, 447
Santolaya-Rey, A. E., Puls, J., & Herrero, A. 1997, A&A, 323, 488
Schaller, G., Schaerer, D., Meynet, G., & Maeder, A. 1992, A&AS, 96, 269
Schild, R. E., Hiltner, W. A., & Sanduleak, N. 1969, ApJ, 156, 609
Schild, R. E., Neugebauer, G., & Westphal, J. A. 1971, AJ. 76. 237
Schilt, J., & Jackson, C. 1952, AJ, 56, 209
Schmidt, G. D., Elston, R., & Lupie, O. L. 1992, AJ, 104, 1563
Schulte, D. H. 1958, ApJ, 128, 41
Schulz, A., & Lenzen, R. 1983, A&A, 121, 158
Scuderi, S., Panagia, N., Stanghellini, C., Trigilio, C., & Umana, G. 1998, A&A, 332, 251
Searle, S. C., Prinja, R. K., Massa, D., & Ryans, R. 2008, A&A, 481, 777
Sharpless, S. 1957, PASP, 69, 239
Simón-Díaz, S., & Herrero, A. 2007, A&A, 468, 1063

Skrutskie, M. F., Cutri, R. M., Stiening, R., et al. 2006, AJ, 131, 1163
Slettebak, A. 1956, ApJ, 124, 173
Sloan, G. C., Kraemer, K. E., Price S. D., & Shipman, R. F. 2003, ApJS, 147, 379
Smith, N., & Conti, P. S. 2008, ApJ, 679, 1467
Sneden, C., Gerhz, R. D., Hackwell, J. A., York, D. G., & Snow, T. P. 1978, ApJ, 223, 168
Souza, S. P., & Lutz, B. Y. 1980, ApJ, 235, L87
Stahl, O., Kaufer, A., & Tubbesing, S. 1999, in Optical and infrared spectroscopy of circumstellar matter, ed. E. W. Guenther, B. Stecklum, & S. Klose (San Francisco, CA: ASP), ASP Conf. Ser., 188, 331
Stahl, O., Jankovics, I., Kovács, et al. 2001, A&A, 375, 54
Stahl, O., Gang, T. Sterken, C., et al. 2003, A&A, 400, 279
Stein, W. A., & Gillettt, F. C. 1971, Nature, 233, 72
Sterken, C. 1977, A&A, 57, 361
Sterken, C., & Wolf, B. 1978, A&A, 70, 641
Sterken, C., de Groot, M., & van Genderen A. M. 1997, A&A, 326, 640
Sterken, C., Arentoft, T., Duerbeck, H. W., & Brogt, E. 1999, A&A, 349, 532
Torres-Dodgen, A. V., Tapia, M., & Carroll, M. 1991, MNRAS, 1991, 249, 1
Urbaneja, M. A., Herrero, A., Kudritzki, R.-P., et al. 2005, ApJ, 635, 311
van Breda, I. G., & Whittet, D. C. B. 1977, Ap&SS, 48, 297
Vidal, N. V. 1973, ApJ, 186, L81

Voelcker, K. 1975, A&AS, 22, 1
Walborn, N. R. 1971, ApJS, 23, 257
Walborn, N. R. 1975, PASP, 87, 759
Walborn, N. R. 1980, ApJS, 44, 535
Walborn, N. R., & Fitzpatrick, E. L. 1990, PASP, 102, 379
Walborn, N. R., Stahl, O., & Gamen, R. C. 2008, ApJ, 683, L33
Waldron, W. L., Corcoran, M. F., Drake, S. A. & Smale, A. P. 1998, ApJS, 118, 217
Wellstein, S., & Langer, N. 1999, A&A, 350, 148
Wendker, H. J., & Altenhoff, W. J. 1980, A&A, 92, L5
Westerlund, B. 1959, PASP, 71, 156
White, R. L., & Becker, R. H. 1983, ApJ, 272, L19
Whittet, D. C. B., van Breda, I. G., & Glass, I. S. 1976, MNRAS, 177, 625
Whittet, D. C. B., Martin, P. G., Hough, J. H., et al. 1992, ApJ, 386, 562
Whittet, D. C. B., Boogert A. C. A., Gerakines, P. A., et al. 1997, ApJ, 490, 729
Wisniewski, W. Z., Wing, R. F., Spinard, H., & Johnson, H. L. 1967, ApJ, 148, L29
Wolf, B., & Stahl, O. 1985, A&A, 148, 412
Woźniak, P. R., Vestrand, W. T., Akerlof, C. W., et al. 2004, AJ, 127, 2436
Zappala, R. R. 1970, in Proc. Conference on Late Type Stars, ed. G. W. Lockwood, & H. M. Dyck (Kitt Peark Contr. No. 554, Lick Obs. Bull. No. 610)

Appendix A: Summary of historical data for Galactic BHGs

In order to understand the role of the BHG phase in the lifecycles of massive stars it is invaluable to contrast the long term (in)stability of such stars to other, potentially related evolutionary phases such as the LBVs. In order to accomplish this we undertook a literature review of all known Galactic examples. This has allowed the construction of the comprehensive spectroscopic and photometric datasets used in the quantitative modeling descibed in Sect. 4. To the best of our knowledge there are 16 known or candidate BHGs within the Galaxy, of which 8 have early (B1-4) spectral types. In constructing this list we have explicitly included 3 high luminosity stars of late-B spectral type which, although classified as luminosity class Iae, have prominent Balmer emission lines that appear characteristic of *bona fide* BHGs.

A.1. The early-B HGs: Cyg OB2 #12

A.1.1. Photometric variability

Gottlieb & Liller ([1978](#)) provide an extensive optical photometric history for Cyg OB2 #12, comprising, where available, annual mean B band magnitudes from ~1890–1980. They report low level annual variability ($m_B \sim 14.5{-}15.0$ mag.) albeit with no apparent secular evolution. Despite being somewhat limited, the compilation of multi-epoch *UBVRIJHK* photometry presented in Table A.1 is consistent with little photometric activity being present[9].

While systematic photometric monitoring of Cyg OB2 #12 ceased after 1980 – fortuitously at a point when spectroscopic observations increased in frequency (Sect. A.1.2) – two further long-term photometric datasets are available. The first, acquired via the HIPPARCOS mission (ESA [1997](#); Perryman et al. [1997](#)), provides data from 1989 November to 1993 March, with the passband, H_p, spanning 3400–9000 Å (van Leeuwen et al. [1997](#)). Subsequently, the Northern Sky Variability Survey (NSVS; Woźniak et al. [2004](#)) yielded a further year long dataset (1999 April–March 2000); this operated without filters, resulting in a wide optical band with a response defined by that of the CCD, extending from 450 to 1000 nm.

These data are summarised in Fig. [3](#) and although the nonstandard passbands do not allow a direct comparison to previous data they do constrain variability over the periods in question. As with the results of Gottlieb & Liller ([1978](#)), these datasets indicate that low level (~0.3 mag) non secular and aperiodic variability is present, which occurs over rather short (~days) timescales.

While only single epoch mid-IR observations are available (Table A.2), multiple epochs of radio continuum observations are available in the literature, and are summarised in Table A.3. While the spectral indices derived from these data are consistent with thermal emission from a partially optically thick stellar wind, these fluxes demonstrate significant variability. As with the short period photometric variability, a possible interpretation of this behaviour is provided in Sect. 3.

---

[9] We note that in common with early observations of all the BHGs considered, interpretation is complicated by the lack of a reported date for some observations – a problem also present for the spectroscopic observations.

A.1.2. Spectral classification and variability

A summary of the multiwavelength spectroscopy obtained for Cyg OB2 #12 over the past half century is presented in Table A.4. The spectral classifications given are those reported by the works in question; reclassification is provided only for those occasions where the source papers assumed an earlier result (this being the case for the IR studies, where Cyg OB2 #12 was typically included as a spectral standard). Regarding reclassification, a luminosity class of Ia$^+$ is implictly assumed throughout the following discussion.

4–6000 Å: Souza & Lutz ([1980](#)), Massey & Thompson ([1991](#)), Klochkova & Chentsov, ([2004](#)) and Kiminiki et al. ([2007](#)) all provide a detailed discussion of the classification of Cyg OB2 #12 from 4000–5000 Å spectra at high resolution and S/N, using the He I 4471 Å:Mg II 4481 Å line ratio as the primary spectral-classification criterion. Following this methodology, spectral types in the range B3–B8 have been inferred by these authors, with variability in the line ratio (e.g. Kiminiki et al. [2007](#)) taken as evidence for changes in the *spectral type* of Cyg OB2 #12.

However, we caution that extreme care must be taken in inferring changes in the *physical properties* of the star from this diagnostic. Firstly, the Mg II 4481 Å transition shows a dependence on stellar luminosity and so callibrations of spectral type versus the He I 4471 Å:Mg II 4481 Å line ratio derived from lower luminosity stars may not a priori be directly applied to Cyg OB2 #12. More critically and as demonstrated in Sect. 4.1, this ratio is highly sensitive to the properties of the photosphere/wind transitional zone. Consequently, changes in the structure of the inner wind – which we may infer from line profile variability in Hα (see below) – at *constant stellar temperature* will cause this line ratio to vary, and in turn lead to the erroneous conclusion that because the spectral type has varied then the *temperature has also changed*.

Given the quality of their spectra – and in conjunction with data presented in Walborn & Fitzpatrick ([1990](#)) – Kiminki et al. ([2007](#)) also employed the weak absorption feature at ~4542 Å as a classification criterion, which they attributed to a blend of He II and Fe II. While an absorption feature at ~4542 Å is observed in B1.5–4 supergiants, it is unlikely to be due to He II (seen only for B0 and earlier supergiants) or Fe II (B5 and later). Given these uncertainties, we instead choose to employ the Si III 4552 Å/Si II 4128 Å line ratio as a primary temperature diagnostic. Thus, upon consideration of the above, we suggest a spectral classification of B5 for the 1992 July 22 spectrum and B4 for the 1998 August, 2000 September and 2008 July spectra (Fig. A.1), noting that the marginally later classification in 1992 is likely to be a result of the lower S/N and spectral resolution of these data. We thus find no evidence for changes in the spectral type of Cyg OB2 #12 in these data.

6–8000 Å: the spectral region surrounding Hα is largely devoid of classification criteria (e.g. Negueruela et al. [2010](#)). However (i) the strong central Hα emission peak superimposed on broad emission wings; (ii) lack of He II 6527, 6683 Å absorption; (iii) absence of S IV 6668, 6701 Å emission; and (iv) the presence of strong C II 6578, 6582 Å photospheric lines are

uniformly present in spectra from 1992 onwards[10] and are all consistent with a highly luminous B supergiant (Fig. 1). As found by Klochkova & Chentsov (2004), the central peak of the Hα profile appears to be variable at low projected velocities (≤ 140 km s^{-1}).

8–9000 Å: despite spanning a period of over 16 years, the 3 I band spectra are essentially identical (a representative spectrum from 2008 is presented in Fig. A.2). To classify Cyg OB2 #12 from these data we employed the scheme described in Negueruela et al. (2010), supplemented by spectra of other early-mid BSGs and BHGs of known spectral type. While the BHG spectra show a similar morphological progression to those of normal BSGs (Negueruela et al. 2010, Fig. A.2), there is no indication of emission in the Paschen series (noting that the lower Balmer transitions are seen in emission). While such a finding precludes the separation of BHGs from BSGs in the spectroscopic window in which GAIA – the Global Astrometric Interferometer for Astrophysics – will operate, the lack of wind contamination aids in the quantitative determination of the underlying stellar parameters (Sect. 4).

Regarding the classification of Cyg OB2 #12, the presence of N I absorption lines indicates a spectral type of B3 or later, with their comparative weakness favouring B3. This finding is consistent with both the strength of the O I 8446 Å line, which clearly lies between B2.5Ia and B4Ia (see Fig. A.2), and the temperature sensitive Pa15/Pa11 and Pa16/Pa11 line ratios. However, the differences between B3 and B4 Ia stars are small – hence we suspect that the slight discrepancies between classifications based on the ~4–5000 Å and ~8–9000 Å windows evident for data obtained in 1992 and 2008 are unlikely to be real. Likewise, distinguishing between B5 and B8 supergiants on the basis of I band spectra alone is particularly difficult (Negueruela et al. 2010); hence we caution against using the results of Sharpless (1957) and Zappala (1970) as evidence for spectroscopic variability prior to 1970. Echoing Sect. 4, changes in the physical properties of the photosphere/wind transitional zone have negligible impact on the I band spectral morphology – hence explaining potential discrepancies between the spectral type of Cyg OB2 #12 determined from the I band and the He I 4471 Å:Mg II 4481 Å diagnostic.

0.98–1.10 μm: two epochs of observations from 1990 and 1992 are presented by Conti & Howarth (1999), who report no variability between the spectra. Unfortunately a paucity of spectral features and little calibration data complicate classification from these data, although the presence of weak He I 1.031 μm suggests a classification of B8 Ia$^+$ or earlier and the absence of He II 1.0124 μm provides an upper limit of B3 Ia$^+$. Such a result is consistent with that derived from our spectra obtained on 1992 July 22.

1.66–1.72 μm: a single epoch of H band spectroscopy was presented by Hanson et al. (1998), with Br11 and He I 1.700 μm lines in absorption and of ~equal strength and He II 1.693 μm

absent. The lack of He II 1.693 μm is characteristic of a B spectral type, with EW(Br11) $\geq$ EW(He I) occuring for B1.5 Ia$^+$ and later (at the resln. of the spectrum in question) and only becoming $\gg$1 at B8 Ia$^+$, hence providing upper and lower limits to the spectral type (Hanson et al. 1998; 2005).

2.0–2.4 μm: Hanson et al. (1996) present a K band spectrum from 1994, in which Brγ and He I 2.112 μm are seen in absorption. For a star of the expected luminosity of Cyg OB2 #12 and with the low S/N and resolution of the data in question, only broad constraints are possible, with the lack of He II 2.189 μm and the presence of He I 2.112 μm implying a classification between B0-9 Ia.

2.35–4.10 μm: finally, Lenorzer et al. (2002) and Whittet et al. (1997) present 2.35–4.1 μm spectra, which we may supplement with an additional spectrum from 1996 April 4. All four display emission in Brα, Pfα and β, with the higher transitions seen in absoprtion. No variability is apparent between any of these spectra; hence we do not reproduce them here. Unfortunately, as with the ~1–2 μm window, there is a dearth of classification features in this region and we may only infer a spectral type between B3-9 Ia$^+$ from the presence and strength of the Brackett and Pfund series and the lack of He I photospheric lines.

To summarise – we find that the available data provides no substantive evidence for the long-term evolution of the spectral type of Cyg OB2 #12 over the past half century, although this conclusion is necessarily weaker prior to the 1990 s, given the sparser dataset available. Nevertheless, this finding is entirely consistent with the long-term lightcurve. A classification of B3-4 Ia$^+$ appears appropiate throughout this period, although short term variability is present in both wind (e.g. Hα...δ) and photospheric lines (e.g. Kiminki et al. 2007).

Both phenomena are common in other luminous B super-/hypergiants (e.g. Clark et al. 2010) where they are assumed to be due to, respectively, time-dependent wind structure and photospheric pulsations resulting in changes in photospheric temperature. Regarding the latter, changes in the He I 4471 Å:Mg II 4481 Å flux ratio have led to the conclusion that the spectral type is variable (B3-8 Ia$^+$), from which changes in the photospheric temperature (16–12 kK) of Cyg OB2 #12 have been *inferred*; such a range is fully consistent with models of the pulsating B supergiant HD 64760 (Kaufer et al. 2006) and the BHGs Wd1-7 and 42 (Clark et al. 2010). However we caution that the detailed non-LTE model atmosphere analysis reveals that variation in the physical structure of the photosphere/wind transitional zone can also lead to this behaviour; hence concluding that the photospheric temperature has been variable based on the current spectroscopic dataset is clearly premature.

A.2. The early-B HGs: ζ^1 Sco

A.2.1. Photometric variability

Sterken (1977) and Sterken et al. (1997) have previously undertaken long-term(differential) *uvby* Stromgren and V *BLUW* photometric campaigns between 1973–1974 and 1982−1995 respectively. They report low level ($\Delta m \sim 0.01$ mag) quasi-periodic variability over a wide range of timescales (~16.5−~2000 days), with additional stochastic variability

---

[10] The low resolution and S/N of previously published spectra are insufficient to comment on the presence, or otherwise, of photospheric features.

($\Delta m \sim 0.05$ mag) superimposed. (Aperiodic) low level ($\Delta m = 0.08$ mag) photometric variations were also present in the Hipparcos dataset between 1989–1993 (Lefèvre et al. 2009) and between 1979–1980 (Burki et al. 1982).

In addition to these data Sterken et al. (1997) also present historical observations from the 10th–19th Century, to which we may add a number of more recent data from the 20th Century (Table A.1). Sterken et al. (1997) suggest that ζ^1 Sco is a long-term variable, reporting $m_V \sim 2.8$ in the middle of the 18th Century, $m_V \sim 4.3$ and 5.4 in 1875 and 1878 and $m_V \sim 4.5-4.8$ between 1890–1900. The latter values are broadly consistent with the photometric data presented in Table A.1, which span the 20th Century and provide no evidence for the long term secular variability that characterises e.g. the LBV phase. Moreover, these data also demonstrate that the near-IR continuum is similarly stable, albeit over a shorter, ~ 30 yr baseline. We therefore conclude that the sole evidence for significant ($\Delta m_V > 0.3$ mag) variability is provided by historical visual estimates dating from before ~ 1890, for which we are unfortunately unable to quantify the observational uncertainty.

Finally, we turn to the radio data, for which Bieging et al. (1989) report possible variability. This mirrors the findings for Cyg OB2 #12 and we provisionally associate this behaviour with the same physical cause (Sect. 3).

A.2.2. Spectroscopic classification and variability

Given the brightness of ζ^1 Sco, spectroscopic observations dating from the turn of the 19th Century are reported in the literature, although a lack of accurate dates for the earlier observations complicates their interpretation. Nevertheless, a summary of these observations are presented in Table A.5; we note that the lower reddening to ζ^1 Sco facilitates a more homgeneous dataset of blue end spectroscopy in comparison to Cyg OB2 #12. Fortuitously, the period between 1900–1950 is well sampled and hence complements the sparse photometric dataset in this period.

This compilation reveals an absence of long-term variability or secular evolution of spectral type over a ~ 110 yr interval. The description of the main features of the optical spectra over this whole period are remarkably consistent; the spectra presented in Fig. A.1 for the period 1994–2009 demonstrating this stability. Nevertheless, numerous authors report line profile variability in the wind dominated P Cygni profile of Hα and β, with the higher H I transitions repeatedly varying between emission and absorption over at least a ~ 50 yr interval (cf. Table A.5 and refs. therein). Rivinius et al. (1997) report the rapid variability of both photospheric *and* wind lines between 1992–1995; we consider it likely that the variability observed in the Hα P Cygni line between 1998–2009 (Fig. 1) reflects a continuation of this behaviour.

A.3. The early-B HGs: HD 190603

Unfortunately, photometric datasets for HD 190603 are somewhat sparse in comparison to the previous two stars, with no photometric observations reported over the last decade and a >16 yr gap in the 1980s–1990s (Table A.1). Nevertheless, we find no evidence for secular variability over the ~ 46 yr period from 1952–1998. Conversely, rapid photometric variability has been reported on several occassions by both Percy & Welch (1983) and Koen & Eyer (2002).

Likewise comparatively few spectral observations have been reported, a problem exacerbated by the lack of reduced spectra

being presented. Consequently we are forced to simply present the spectral classifications reported for HD 190603 in Table A.6. These data indicate a corresponding lack of spectroscopic evolution over a 50 year period. Indeed, the description of the spectrum by both Beals (1946) and Merrill & Birwell (1943) as, respectively, that of a P Cygni supergiant and a Be star, suggest a similar morphology prior to 1933. The latter authors further described variable emission lines; similar findings being reported by Rosendhal (1973) and Rivinius et al. (1997).

A.4. The early-B HGs: HD 80077, HD 169454 and BP Cru

We next turn to the remaining early-B HGs. We refrain from tabulating their sparse photometric datasets but note that there is no evidence for secular variability in any of the three stars; for instance comparison of the optical (Hiltner 1956; Kilkenny et al. 1993) and near-IR (Whittet et al. 1997; Skrutskie et al. 2006) data for HD 169454 reveal constancy over ~ 35 and ~ 26 yr intervals respectively. However, following the previous discussions, rapid, low amplitude photometric variability appears ubiquitous (van Leeuwen et al. 1998; Sterken 1977 and Hammerschlag-Hensberge et al. 1979, respectively).

As with HD 190603, Table A.6 summarises their spectral types as reported in the literature. No evidence for the long-term (secular) evolution of spectral type over timescales in excess of 30 yrs was found, with the description of HD 169454 as a B star with H I P Cygni emission lines (Merrill & Burwell 1943) suggesting spectral stability for nearly a century. In contrast line profile variability (LPV) on a timescale of days-weeks is present in all 3 stars (Knoechel & Moffat 1982; Rivinius et al. 1997; Kaper et al. 2006, respectively).

A.5. The early-BHGs/WNVL stars Wd1-5 and 13

The remaining early-B HGs are found within the massive young cluster Wd1, and on the basis of a restricted wavelength range (5800–8900 Å) were classified as borderline BHG/very late WN stars, forming an evolutionary sequence from Wd1-5 through –13 to the WN9h star Wd1-44 (Clark et al. 2008). Unfortuntely, these stars have only been observed over the past $\sim$decade, but no evidence for long term variability has been found (Clark et al. 2010). However, Wd1-13 is a confirmed ~ 9.27 day massive binary, while pronounced LPV in Wd1-44 also argues for such an identification. Consequently, we suspect that all three stars to have formed as the result of close binary evolution.

A.6. The late-B HGs

Finally, we examine the eight BHGs with spectral types of B5 and later that have been identified within the Galaxy. Three – W7, W33 (both B5 Ia$^+$) and W42a (B9 Ia$^+$) – are located within the massive young cluster Wd 1 and are discussed in detail in Clark et al. (2010). Unfortunately, the long-term spectroscopic and photometric datasets for these stars are less complete than those of the early-B HGs described above, although they are sufficient to confirm the presence of rapid LPV. This behaviour, as well as short term low amplitude photometric pulsations is also present in the other examples; HD 160529 (A9-B8 Ia$^+$; Stahl et al. 2003), HD 168607 (B9 Ia$^+$; Chentsov et al. 2003, Sterken et al. 1999), HD 168625 (B8 Ia$^+$; Sterken et al. 1999; Chentsov et al. 2003), HD 183143 (B7 Iae; Adelman et al. 2000; Chentsov et al. 2003) and HD 199478 (B8 Iae; Percy et al. 2008; Markova & Valchev 2000), suggesting that

the α Cygni instabilities are ubiquitous across the complete temperature and luminosity range spanned by BHGs.

This phenomenon is also found to extend to cooler temperatures, having been identified in a number of early-A (A0-2.5 Ia$^+$/Iae) stars with similar spectral morphologies to the BHGs – e.g. HD 92207 (A0 Iae; Sterken 1977; Kaufer et al. 1997), HD 223385 (A2.5 Ia$^+$; Adelman & Albayrak 1997; Chentsov 2003) and AS 314 (A0 Ia$^+$; Miroshnichenko 2000).

However, unlike the early-B HGs, HD 160529 and 168607 demonstrate characteristic LBV photometric modulation, with the former also exhibiting correlated spectral type variability, while both HD 168625 and HD 92207 show evidence for a complex, dusty circumstellar environment (Roberto & Herbst 1998; Clarke et al. 2005) implying recent enhanced mass loss, possibly associated with an LBV phase.
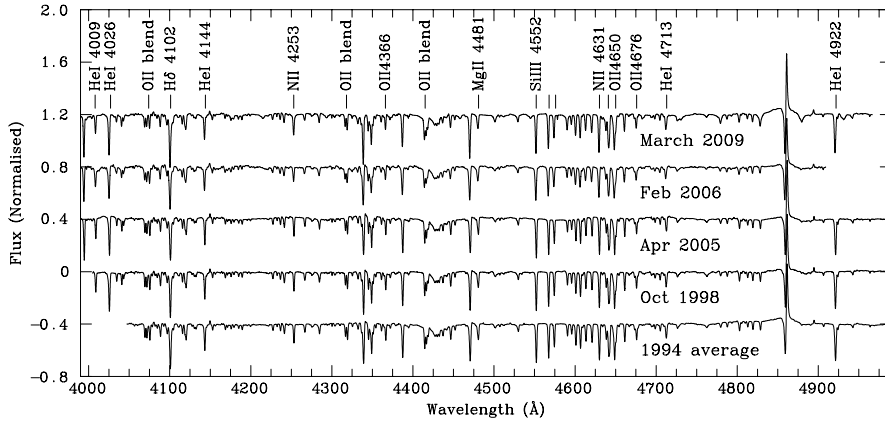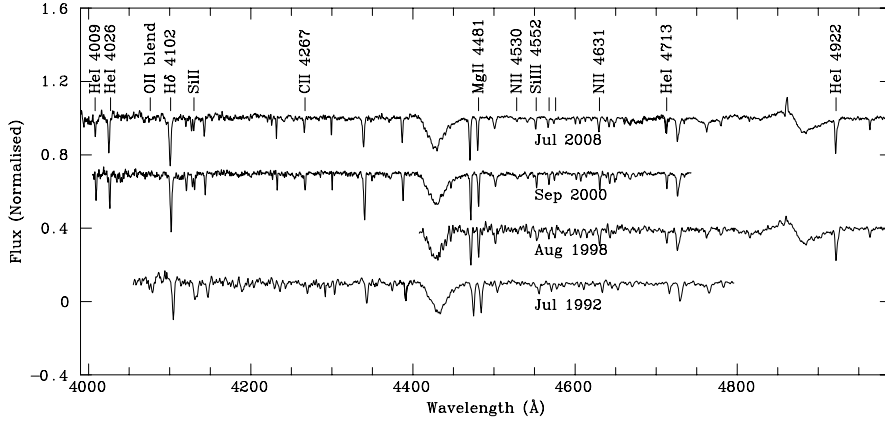
Fig. A.1. Long-term evolution of Cyg OB2 #12 (1992–2008; *top panel*) and ζ^1 Sco (1998–2009; *bottom panel*) in the ~4000–4800 Å spectral region, encompassing the Si III 4552 Å/Si II 4128 Å temperature diagnostic.
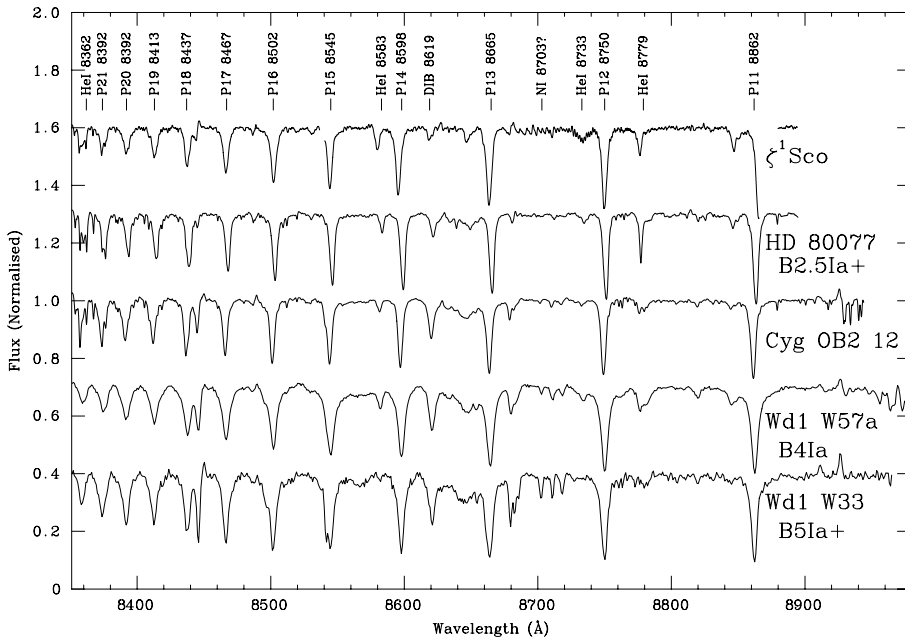
Fig. A.2. Comparison of the *I* band spectra of Cyg OB2 #12 and ζ^1 Sco with other galactic BHGs. Note the systematic weakening of He I and strengthening of N I transitions with decreasing temperature, which permit spectral classification in whis wavelength range.

Table A.1. Summary of historical photometric magnitudes used to construct the optical-near IR SEDs, ordered by time.

| Date	U	B	V	R	I	J	H	K	Reference
Cyg OB2 #12									
<1954	16.67 ± 0.1	14.66 ± 0.04	11.47 ± 0.04	–	–	–	–	–	Sharpless (1957)
<1962	17.21	14.71	11.49	8.36	6.20	4.55	–	2.81	Johnson & Borgman (1963)
<1964	17.20 ± 0.01	14.70 ± 0.01	11.48 ± 0.01	8.26 ± 0.01	5.94 ± 0.01	4.32 ± 0.01	–	2.66 ± 0.1	Johnson (1965)
<1967	17.15	14.70	11.48	8.26	5.95	4.42	–	2.70	Wisniewski et al. (1967)
<1968	–	–	-	8.26	5.94	4.32	–	2.66	Johnson (1968)
<1971	–	–	–	–	–	–	–	2.60	Stein & Gillett (1971)
<1973	–	–	–	–	–	–	3.34 ± 0.06	2.77 ± 0.05	Chaldu et al. (1973)
1972 Autumn	–	–	–	–	–	4.59 ± 0.05	3.37 ± 0.05	2.82 ± 0.05	Voelcker (1975)
1975–6	–	–	–	–	–	4.38 ± 0.02	3.28 ± 0.02	2.72 ± 0.02	Harris et al. (1978)
1980 Aug. 26	–	–	–	–	–	–	–	2.80 ± 0.01	Abbott et al. (1981)
1981 July	–	–	–	–	–	–	3.33 ± 0.01	2.72 ± 0.01	Leitherer et al. (1982)
1989 May 26–30	17.18 ± 0.01	14.81 ± 0.01	–	–	–	4.39 ± 0.04	3.34 ± 0.04	2.75 ± 0.04	Torres-Dodgen et al. (1991)
1990 June 6	–	–	11.46 ± 0.01	–	–	–	–	–	Massey & Thompson (1991)
1998 June 21	–	–	–	–	–	4.7 ± 0.3	3.5 ± 0.3	2.70 ± 0.4	Skrutskie et al.(2006)
ζ¹ Sco									
<1924	–	–	4.88	–	–	–	–	–	HD catalogue
1949–1952[1]	–	–	4.88	–	–	–	–	–	Schilt & Jackson (1952)
<1954[2]	–	–	4.9	–	–	–	–	–	Bidelman (1954)
<1958	–	–	4.86	–	–	–	–	–	Code & Houck (1958)
<1958	–	5.03	4.3	–	–	–	–	–	Evans et al. (1959)
1958 March–April	4.54	5.20	4.82	–	–	–	–	–	Westerlund (1958)
<1961	–	–	4.80	–	–	–	–	–	Buscombe (1962)
1963	–	–	4.74	–	–	–	–	–	Andrews et al. (1968)
1963 June	4.57	5.19	4.72	–	–	–	–	–	Feinstein (1968)
1964 March	4.64	5.20	4.72	–	–	–	–	–	Feinstein (1968)
1967–68	–	–	4.71	–	–	–	–	–	Schild et al. (1969)
1968 July	–	–	–	–	–	–	3.30	3.11	Schild et al. (1971)
1973	–	–	4.73≤ V ≤4.83	–	–	–	–	–	Jaschek & Jaschek (1973)
1974 April	–	–	–	–	–	3.47 ± 0.03	3.27 ± 0.03	3.11 ± 0.03	Whittet et al. (1997)
1963 to 1976[3]	–	–	4.73	–	–	–	–	–	Feinstein & Marraco (1979)
1979 Apr. to 1980 Sept.[4]	–	–	4.66≤ V ≤4.78	-	–	–	–	–	Burki et al. (1982)
1981 August 9	–	–	–	–	–	–	–	3.14 ± 0.05	Abbott et al. (1981)
1974–82	4.76	5.29	4.77	4.31	3.85	–	–	–	Fernie (1983)
1982 August	–	–	–	–	–	3.58 ± 0.03	3.32 ± 0.03	3.18 ± 0.03	Leitherer & Wolf (1984)
<1984	–	5.18	4.78	–	–	3.53 ± 0.02	3.31 ± 0.02	3.13 ± 0.03	Lopez & Walsh (1984)
<2003	4.61	–	–	–	–	–	–	–	Reed et al. (2003)
1999 May 22	–	–	–	–	–	3.6 ± 0.3	3.3 ± 0.2	3.3 ± 0.2	Skrutskie et al.(2006)
HD 190603									
1952–4	5.72	6.18	5.65	–	–	–	–	–	Hiltner (1956)
<1958	5.59	6.13	5.56	–	–	–	–	–	Golay (1958)
<1961	–	6.14	5.59	–	–	–	–	–	Bouigue et al. (1961)
1962–70	5.66	6.14	5.62	–	–	–	–	–	Crawford et al. (1971)
<1964	5.72 ± 0.01	6.18 ± 0.01	5.65 ± 0.01	5.12 ± 0.01	4.72 ± 0.01	4.50 ± 0.01	–	4.11 ± 0.1	Johnson (1965)

Table A.1. continued.

Date	Waveband								Reference
	U	B	V	R	I	J	H	K	
<1966	5.73	6.19	5.65	–	–	–	–	–	Johnson et al. (1996)
<1968	5.69	6.15	5.60	–	–	–	–	–	Blanco et al. (1968)
<1968	–	6.14	5.62	–	–	–	–	–	Lesh (1968)
1968–9	5.81	6.25	5.70	–	–	–	–	–	Burnichon & Garnier (1976)
1972 Autumn	–	–	–	–	–	4.50 ± 0.05	4.14 ± 0.05	4.11 ± 0.05	Voelcker (1975)
<1974	5.72	6.18	5.64	–	–	–	–	–	Nicolet (1978)
1974 Sept.	–	–	–	–	–	4.43 ± 0.03	4.24 ± 0.03	4.10 ± 0.03	van Breda & Whittet (1977)
1974–82	5.64	6.13	5.56	5.01	4.62	–	–	–	Fernie (1983)
1975 Oct.	–	–	–	–	–	–	–	4.1 ± 0.2	Sneden et al. (1978)
1976–78	–	6.18 ± 0.02	5.63 ± 0.02	5.08 ± 0.02	4.71 ± 0.02	–	–	–	Moffett & Barnes (1979)
1979–82	–	6.18	5.64	–	–	–	–	–	Percy & Welch (1983)
1998 May 11	–	–	–	–	–	4.42 ± 0.26	4.26 ± 0.20	4.04 ± 0.03	Skrutskie et al. (2006)

Notes. Where available errors and exact dates of observations are presented. For brevity we have not replicated the B band lightcurve of Gottlieb & Liller (1978) for Cyg OB2#12 here. Observations between 1945–1951 by Cousins (1952) suggest that ζ^1 Sco was variable with low amplitude ($\Delta m = 0.05$ mag) between 1945–1951, although details of the filter set used are not described. Sterken (1977) report 35 epochs of differential $ubvy$ photometry between 1973–1974 for ζ^1 Sco, with a further 399 epochs between 1982–1995 presented by Sterken et al. (1997); throughout these periods minimal variability was observed ($\Delta ubvy \leq 0.1$ mag.). Finally Percy & Welch (1983) report 52 epochs of BV band photometry between 1979 May 30 and 1982 July 1 indicating t to be a short period variable. [1] 3 observations in this period; no details of band pass. [2] Phot. magnitude possibly sourced from HD catalogue? [3] 3 observations over this period. [4] 43 observations over this period.

Table A.2. Summary of mid- to far-IR fluxes used to construct the SEDs.

Wavelength (μm)	Magnitude	Reference
Cyg OB2 #12		
2.30	2.72 ± 0.01	Leitherer et al. (1982)
2.345	2.635 ± 0.02	Harris et al. (1978)
3.013	2.405 ± 0.02	Harris et al. (1978)
3.108	2.375 ± 0.02	Harris et al. (1978)
3.420	2.281 ± 0.02	Harris et al. (1978)
3.45	2.37 ± 0.05	Abbott et al. (1981)
3.50	2.28 ± 0.05	Chaldu et al. (1973)
3.57	2.28 ± 0.02	Leitherer et al. (1982)
3.57	2.170 ± 0.05	Torres-Dodgen et al. (1991)
3.58	2.217 ± 0.02	Harris et al. (1978)
3.820	2.178 ± 0.02	Harris et al. (1978)
4.29	2.057 ± 0.118	MSX (Egan et al. 2001)
4.80	2.37 ± 0.10	Abbott et al. (1981)
4.97	2.06 ± 0.02	Leitherer et al. (1982)
8.28	1.946 ± 0.044	MSX (Egan et al. 2001)
10.2	2.03 ± 0.10	Abbott et al. (1981)
10.9	1.95 ± 0.07	Leitherer et al. (1982)
12.0	1.642 ± 0.00	IRAS PSC (1985)
12.13	1.900 ± 0.056	MSX (Egan et al. 2001)
14.65	1.713 ± 0.067	MSX (Egan et al. 2001)
20.0	1.54 ± 0.10	Abbott et al. (1981)
21.34	1.575 ± 0.079	MSX (Egan et al. 2001)
25.0	1.204	IRAS PSC (1985)
ζ^1 Sco		
3.45(L)	2.98 ± 0.03	Leitherer & Wolf (1984)
4.7(M)	2.90 ± 0.03	Leitherer & Wolf (1984)
8.28	2.624	MSX (Egan et al. 2001)
12.13	3.416	MSX (Egan et al. 2001)
14.65	3.560	MSX (Egan et al. 2001)
HD 190603		
3.6	3.96 ± 0.18	Sneden et al. (1978)
4.9	3.89 ± 0.20	Sneden et al. (1978)
8.28	3.68 ± 0.04	MSX (Egan et al. 2001)
9.0	3.12 ± 0.01	AKARI
12.13	3.47 ± 0.08	MSX (Egan et al. 2001)
14.65	3.46 ± 0.09	MSX (Egan et al. 2001)

Table A.3. Summary of mm and radio fluxes in mJy used to construct the SEDs, ordered by time.

Date	Waveband									Reference
	0.13 cm	0.7 cm	1.3 cm	2 cm	3.5 cm	3.6 cm	6.1 cm	6.2 cm	20.5 cm	
Cyg OB2 #12										
1980 March 22	–	–	21 ± 3	–	–	–	–	–	–	Wendker & Altenhoff (1980)
1980 May 22+23	–	–	–	–	–	–	–	3.2 ± 0.3	–	Abbott et al. (1981)
1981 Oct. 16	–	–	–	6.0 ± 2.0	–	–	–	3.4 ± 0.2	–	Bieging et al. (1989)
1982 March 27	–	–	–	4.5 ± 0.3	–	–	–	–	–	White & Becker (1983)
1982 Aug. 26	–	–	–	–	–	–	–	2.2 ± 0.2	2.0 ± 0.2	Bieging et al. (1989)
1983 Aug./Oct.	–	–	–	–	–	–	–	–	2.1 ± 0.3	Becker & White (1985)
1993 May 1	–	–	–	–	–	6.06 ± 0.07	3.94 ± 0.07	–	–	Waldron et al. (1998)
1994 Sept.	–	–	–	7.7 ± 0.3	4.74 ± 0.14	–	–	4.00 ± 0.20	–	Scuderi et al. (1998)
1994 Oct.	–	–	–	12.0 ± 0.2	7.40 ± 0.08	–	–	4.00 ± 0.20	–	Scuderi et al. (1998)
1995 April 27	–	22.9 ± 0.6	–	11.3 ± 0.1	7.18 ± 0.04	–	3.64 ± 0.12	–	–	Contreras et al. (1996)
1999 June 28	–	22.9 ± 0.6	–	9.0 ± 1.5	5.9 ± 0.1	–	4.2 ± 0.1	–	–	Contreras et al. (2004)
ζ¹ Sco										
1981 May 7	–	–	–	–	–	–	1.2 ± 0.3	–	–	Bieging et al. (1989)
1984 March 9	–	–	–	–	–	–	2.0 ± 0.2	–	–	Bieging et al. (1989)
1984 April 3	–	–	–	4.3 ± 0.1	–	–	1.9 ± 0.2	–	–	Bieging et al. (1989)
1990 Sept. 12–14	23.0 ± 2.4	–	–	–	–	–	–	–	–	Leitherer & Robert (1991)
<2006	–	–	–	–	–	2.4	–	–	–	Benaglia et al. (2007)
HD 190603										
1979 July 13	–	–	–	–	–	–	<0.5	–	–	Abbott et al. (1981)
1994 Oct.	–	–	–	0.7 ± 0.2	0.7 ± 0.1	–	–	0.58 ± 0.06	–	Scuderi et al. (1998)

Notes. For brevity the wavelengths are presented to the nearest 0.1 cm, with exact values given in the papers in question.

Table A.4. Summmary of historical spectral observations of Cyg OB2 #12.

Date	Wavelength	Spectral type	Comments	Reference
≤1954	*4100–6600 Å*	*<A0 I*	*Hα in emission*	Morgan et al. ([1954](#))
≤1957	8–9000 Å	*B5 Ia*	–	Sharpless ([1957](#))
≤1970	*near IR*	*B8 Ia⁺*	–	Zappala ([1970](#))
≤1971	*?*	*–*	*Hα in emission*	Bromage ([1971](#))
≤1973	5–8700 Å+ 8–11 000 Å	*–*	Hα in emission	Chaldu et al. ([1973](#))
1977 July	3840–4480 Å +Hα	B8 Ia⁺	Variable Hα in emission	Souza & Lutz ([1980](#))
1980 Autumn	*Hα*	*–*	*Hα in emission*	Leitherer et al. ([1982](#))
≤1981	*4000–6600 Å*	*–*	*Hα+Hβ in emission*	Hutchings ([1981](#))
1989–90 summer + "few years earlier"	*encompasses Hα + ~4089–4686 Å*	B5 Ia B5 Ia	Hα+Hβ in emission, Hγ+Hδ infilled	Massey & Thompson ([1991](#))
1990 August	0.98–1.10 μm	>B3 Ia,<B8 Ia	–	Conti & Howarth ([1999](#))
1992 July	0.98–1.10 μm	>B3 Ia, <B8 Ia	–	Conti & Howarth ([1999](#))
1992 July 17	**4036–4836 Å** **5765–9586 Å**	**B4-5 Ia** **B3 Ia**	**Hγ+Hδ in absorption** **Hα in emission**	**This work**
1994 Sept.	2–2.2 μm	>B0.5 Ia, <B9 Ia	–	Hanson et al. ([1996](#))
1995 July 17	**6366–6772 Å**	**–**	**Hα in emission**	**This work**
1995 Dec. 23	2.35–8 μm	>B3 Ia, <B9 Ia	Brα, Pfα+β in emission	Whittet et al. ([1997](#))
1996 April 4	**2.35–8 μm**	**>B3 Ia, <B9 Ia**	**Brα, Pfα+β in emission**	**This work**
1996 Oct. 17	2.35–8 μm	>B3 Ia, <B9 Ia	Brα, Pfα+β in emission	Whittet et al. ([1997](#))
1997 June	1.66–1.72 μm	>B1.5 Ia, <B8 Ia	–	Hanson et al. ([1998](#))
1998 Apr.–May	2.35–8 μm	>B3 Ia, <B9 Ia	Brα, Pfα+β in emission	Lenorzer et al. ([2002](#))
1998 Aug. 09	**3940–5737 Å** **6366–6772 Å**	**B4 Ia** **–**	**Hβ in emission** **Hα in emission**	**This work**
1999 July 10	5500–7700 Å	B Ia	Hα in emission	Kiminki (2010, priv. comm.)
2000 July 10	5500–7700 Å	B Ia	Hα in emission	Kiminki (2010, priv. comm.)
2000 Sept. 18	3600–5200 Å	B3 Iae	Hβ infilled	Kiminki et al. ([2007](#))
2000 Sept. 23	**4000–4750 Å** **6340–6740 Å**	**B4 Ia** **–**	**Hγ+Hδ in absorption** **Hα in emission**	**This work**
2001 June 21	4542–7939 Å	B5 Ia	Balmer line emission	Klochkova & Chenstov ([2004](#))
2001 August 24	3800–4500 Å	B6 Iae	Hγ+Hδ in absorption	Kiminki et al. ([2007](#))
2001 Sept. 01	3800–4500 Å	B8 Iae	Hγ+Hδ in absorption	Kiminki et al. ([2007](#))
2003 April 12	5273–6764 Å	B5 Ia	Hα emission	Klochkova & Chenstov ([2004](#))
2007 Aug. 22	**7600–8900 Å**	**B3 Ia**	-	**This work**
2007 Aug. 30	5600–6800 Å	B Ia	Hα in emission	Kiminki (2010, priv. comm.)
2008 July 22	**4000–5270 Å** **6450–7150 Å** **8350–8900 Å**	**B4 Ia** **–** **B3 Ia**	**Hβ in emission** **Hγ+Hδ in absorption** **Hα in emission**	**This work**

Notes. A parameter is listed in italics if not explicitly given (wavelength of observation) or the data from which it is derived was not presented. Parameters given in bold are from this work. Hα is variable between the two epochs of observations presented by Klochkova & Chenstov ([2004](#)) as Hβ and γ are between the 2000–8 spectra presented here, while Conti & Howarth ([1999](#)) report no variability between 1990–2002 in the ~1 μm region. Selected spectra between 1992–2008 are plotted in Fig. A.1.

Table A.5. Summary of historical spectral observations of ζ^1 Sco.

Date	Wavelength	Spectral type	Comments	Reference
<1896	–	–	*Hβ in emission*	Pickering ([1896](#))
1891–1899	*4000–4900 Å*	B1p	*P Cygni profiles in Hβ, γ all other lines in absorption (He I 4009, O II 4349, C II 4267)*	Cannon ([1901](#))
1924	*4100–4900 Å*	*B(2)eq*	*P Cygni profiles in Hβ, γ Hδ in absorption*	Merrill et al. ([1925](#))
1903–1929	–	*B1e Ia*	–	Bidelman ([1954](#))
1926–1930	*3950–4900 Å*	*B1pe*	–	Rimmer ([1930](#))
30/07/34	–	–	*P Cygni profiles in Hα and D3 He I*	Merril & Burwell ([1943](#))
<1938	–	–	*Listed as variable*	Payne-Gaposchkin & Gaposchkin ([1938](#))
1954–1958	*3800–6600 Å*	B1.5 Ia$^+$	No appreciable difference from Cannon ([1901](#))	Code & Houck ([1958](#))
26/04/58 to 03/09/60[1]	*3900–4500 Å*	*B1e Ia*		Buscombe et al. ([1962](#))
22/08/61	6200–6600 Å	–	*Hα in emission*	Jaschek et al. ([1964](#))
7/08/66	*3800–4700 Å*	*B1 Iae*	*Hβ in emission, Hγ, δ & He I 4471 in absn.*	Buscombe & Kennedy ([1968](#))
6/07/60 9/08/60 10/08/60 28/06/66 27/07/66	3100–6750 Å	B1 Ia	P Cygni profiles in Hα, β & He Iλλ5876, 6678 Remaining lines in absorption Variability in Hα profile, but no global spectral evolution	Hutchings ([1968](#))
<1969	*blue end*	B1.5Ia	–	Schild et al. ([1969](#))
21/04/65, 20/05/67 18/03/68, 14/08/70	3500–4900 Å	B1 Ia$^+$	P Cygni profiles in Hβ, γ Variable He I, N II & O II phot. lines	Jaschek & Jaschek ([1973](#))
6/08/68	*5800–6700 Å*	–	P Cygni profiles in Hα, He Iλλ5876, 6678	Rosendhal ([1973](#))
16/05/73 to 10/07/73	*blue end*	–	*No apparent variability in spec. type*	Hutchings et al. ([1976](#))
28/04/74 to 1/05/74 28/04/75	3800–4400 Å	*B1.5 Ia$^+$*	*No variability above 20% in line strength reported*	Walborn ([1975](#))
1974 Oct. & 1975 Mar.	~Hα	–	Variation in Hα P Cygni profile	Dachs et al. ([1977](#))
26/06/72 to 14/08/75[2]	3400–6700 Å	*B1Ia*	Variable P Cygni profiles in Hα, β & He Iλλ5876, 6678 No secular evolution in spec. type	Sterken & Wolf ([1978](#))
<1984	4300–4900 Å 5500–6800 Å	B1.5 Ia$^+$	Variable P Cygni profiles in Hα, β & He Iλ6678	Lopez & Walsh ([1984](#))
1995[4] 1990 to 1994[3]	3450–8630 Å 4000–6740 Å	B1.5 Ia$^+$	Variable P Cygni profiles in Hα, β, He Iλ 6678 & Fe III Hγ, δ in absorption No changes in He I:Si III ratio & hence spec. type	Rivinius et al. ([1997](#))
1998 Oct. 7	**4000–8950 Å**	**B1.5 Ia$^+$**	**Hα, β, He Iλ 6678 P Cygni, higher Balmer series in absorption**	**This work**
1999 June–July[5]	**4000–8950 Å**	**B1.5 Ia$^+$**	**Hα, β, He Iλ 6678 P Cygni, higher Balmer series in absorption**	**This work**
2002 March–May[6]	5810–7205 Å	–	Variable Hα P Cygni	Morel et al. ([2004](#))
2003 May–June	4000–7000 Å	B1.5 Ia$^+$	–	Crowther et al. ([2006](#))
2005 April 24	**3800–6800 Å**	B1.5 Ia$^+$	**Hα, β & He Iλ6678 P Cygni, higher**	**This work**

Table A.5. continued.

Date	Wavelength	Spectral type	Comments	Reference
			Balmer series in absorption	
2006 Feb. 16	**3933–7985 Å**	**B1.5 Ia$^+$**	**Hα, β & He Iλ6678 P Cygni, higher Balmer series in absorption**	**This work**
2009 March 06	**3060–5600 Å**	**B1.5 Ia$^+$**	**Hβ P Cygni, higher Balmer series in absorption**	**This work**

Notes. A parameter is listed in italics if not explicitly given (wavelength of observation) or the data from which it is derived was not presented. Selected spectra between 1992–2009 are plotted in Fig. A.1. [1] 6 observations in this period, [2] 44 observations in this period, [3] 233 observations in this period, [4] 57 observations in this period, [5] 14 observations in this period. [6] 6 observations in this period.

Table A.6. Summary of the dates of historic spectral classifications of the Galactic BHGs.

Publication	Observation date
HD 80077 (B2.5 Ia⁺)	
Morgan et al. (1955)	1942–1955[a]
Buscombe & Kennedy (1968)	1963–1967[b]
Nordstrom (1975)	<1975[a]
Moffat & Fitzgerald (1977)	<1977[a]
Knoechel & Moffat (1982)	1977[a,b]
Negueruela et al. (in prep.)	2008
HD 169454 (B1 Ia⁺)	
Morgan et al. (1955)	1942–1955[a]
Hiltner (1956)	<1956
Code & Houck (1958)	<1958
Botto & Hack (1962)	<1962
Hutchings (1970)	1968
Wolf & Stahl (1985)	1972–1974
Walborn (1980)	1973–1975
Hutchings (1976)	1973–1975
Rivinius et al. (1997)	1992–1995[b]
Hanson et al. (1996)	1994[c]
Hanson et al. (1998)	1997[c]
Groh et al. (2007)	2001–2004[a]
HD 190603 (B1.5 Ia⁺)	
Morgan et al. (1955)	1942–1955
Ahmad (1952)	<1952
Hiltner (1956)	<1956
Slettebak (1956)	<1956
Lesh (1968)	<1968
Hutchings (1970)	1968
Walborn (1971)	1969
Hutchings (1976)	1973–1975
Bisiacchi et al. (1976)	1975–1976
Andrillat et al. (1995)	1988–1993
Rivinius et al. (1997)	1990–1199[b]
Lennon et al. (1992)	1990
Hanson et al. (1996)	1994[c,d]
Blum et al. (1997)	1996[c,d]
Hanson et al. (1998)	1998[c]
Crowther et al. (2006)	1992–2003
Markova & Puls (2008)	<2007
BP Cru (B1 Ia⁺)	
Vidal (1973)	1973[d]
Bord (1979)	1974
Hammerschlag-Hensberge et al. (1979)	1975
	1977
	1978
Parkes et al. (1980)	1977–1978[d]
Kaper et al. (1995)	1984
Kaper et al. (2006)	1996[b]
	2002[b]

Notes. All classifications made in the optical (4–6000 Å) band unless otherwise noted – [a] marginally earlier spectral type of B2 Iae given. [b] multiple spectra in this period. [c] observations within the near-IR (~1–2.2 μm) window. [d] marginally later spectral type of B1.5 or B2 Iae given.

Appendix B: Spectropolarimetry

Considering a simple "core-halo" wind model for heuristic purposes, electron scattering of photospheric radiation in an asymmetric outflow will generate a grey intrinsic linear polarization, while emission lines formed in the wind will see a smaller scattering optical depth, and so are expected to be less polarized (e.g., McLean 1979). This will result in depolarization through the line, although the addition of an interstellar-polarization vector means that this "line effect" often manifests in other ways, including an observed increase in degree of polarization, P.

Previously unpublished spectropolarimetric observations of Cyg OB2 #12 and ζ^1 Sco were obtained as part of the investigations reported by Harries et al. (2002). Cyg OB2 #12 was observed on 1995 July 17 (using the WHT with ISIS spectrograph; $R \simeq 3300$), and ζ^1 Sco on 1997 Jun. 5 (AAT with RGO spectrograph; $R \simeq 5000$), with the data acquisition and reduction essentially as in the manner described by Harries & Howarth (1996). Results are displayed in Fig. B.1.

For Cyg OB2 #12 there is no compelling evidence of a change in polarization through the Hα emission line (although there is a hint of a possible increase in P), and hence no strong indication of large-scale asymmetry in the electron-scattering envelope. Similarly, there is no strong evidence for temporal polarimetric variability; although the spread in published R-band photopolarimetric measurements is somewhat larger than their quoted *formal* errors, the results presented by Schmidt et al. (1992; $P = 7.893 \pm 0.037\%$, $\theta = 116.23 \pm 0.14°$) Whittet et al. (1992; $7.97 \pm 0.05\%$, $117°$), and Kobulnicky et al. (1994; $8.35 \pm 0.21\%$, $117.8°$) are all broadly consistent with the present results, as are earlier O-band measurements reported by Kruszewski (1971) and by McMillan & Tapia (1977). We note, however, an anomalous result reported by Schulz & Lenzen (1983; $P = 10.05 \pm 0.12\%$, $\theta = 125°$); their observations of two further stars agree well with measurements presented by Schmidt et al. (1992).

In spite of its brightness, ζ^1 Sco has been much less extensively observed, with the only available point of direct comparison being the narrow-band ($\Delta\lambda = 8.5$ Å) Hα polarimetric measurement of $P = 2.39 \pm 0.03\%$, $\theta = 64.6°$ reported by McLean & Clarke (1979)[11]. This is in agreement with our results; however, our spectropolarimetry clearly reveals a significant, ~1.5° position-angle rotation through the emission line.

Physically, the line effect may be associated with large-scale, axisymmetric structures (such as might result from rapid rotation), or irregular "clumps". For a star with parameters similar to those of ζ^1 Sco, summarized in Table 4, the critical equatorial rotation velocity[12] is $v_e \simeq 210$ km s⁻¹. With a measured $v_e \sin i$ of ~45 km s⁻¹ (Table 3), the intrinsic rotation is probably substantially subcritical ($v_e/v_{crit} \lesssim 0.69$ with 95% confidence). A rotationally-induced axisymmetric departure from spherical symmetry (i.e. a "disc" or "polar" wind) therefore seems a priori improbable as the origin of the line effect in this star. A more likely cause of the observed change in polarization is the presence of transient large-scale inhomogenities, or "clumps", as has been proposed for P Cygni and AG Car on the basis of spectropolarimetric observations by e.g. Nordsieck et al. (2001) and Davies et al. (2005); indeed CMFGEN model atmosphere analysis of both these stars confirms the presence of the significant wind clumping (Najarro et al. 2001; Groh et al. 2009a).

---

[11] Matthewson & Ford (1970) report a blue-band measurement of $P = 2.29\%$, $\theta = 67.3°$.

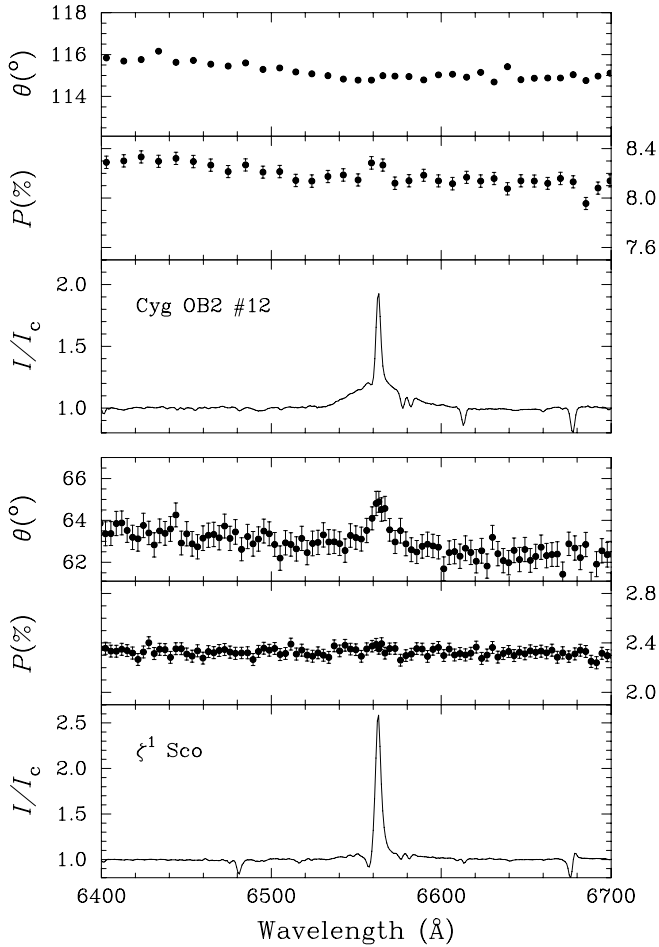[12] The velocity at which the outward centrifugal force equals the inward gravitational force.

Fig. B.1. Linear spectropolarimetry of Cyg OB2 #12 and ζ^1 Sco. Rectified spectra are shown at full resolution; polarimetry is binned to an (almost) constant error of 0.05% in degree of polarization.

Therefore, by direct analogy, an additional observational test of this hypothesis for ζ^1 Sco would be the detection of time-dependent variations in polarization (under the assumption that there is no prefered geometry for the clumping), noting that spectroscopic observations are already strongly indicative of the presence of transient wind structure (Appendix A).

Appendix C: The age of NGC 6231 and Sco OB1

Given its proximity (~1.64 kpc; Sana et al. 2008), NGC 6231, its host association Sco OB1, and the massive stars located within both have been the subject of numerous multiwavelength studies. Here we review these data in order to constrain the evolutionary history of both cluster and association to better understand the nature of ζ^1 Sco. Photometric studies by Baume et al. (1999) suggest a significant age spread within NGC 6231, with star formation apparently commencing ~10 Myr ago, culminating in the formation of the massive stellar cohort ~3−5 Myr ago. The latter age is consistent with the findings of Sana et al. (2006a, 2007), who report a similar value of 2−4 Myr from an analysis of the photometric data of (X-ray selected) pre-MS stars. An analogous study of the wider Sco OB1 association by Perry et al. (1991) supports a non coeval star formation history for this region, yielding an age of $\sim 8^{+4.5}_{-3}$ Myr.

Catalogues of the OB stellar content of both NGC 6231 and Sco OB1 are provided by Sana et al. (2006b) and Ankay et al. (2001) respectively, and allow for the individual placement of stars on the HR diagram presented in Fig. 13. For those stars in Sana et al. we adopted the luminosities given by these authors and utilised the spectral type/temperature relation of Martins et al. (2005). The temperatures and luminosities of the stars in Ankay et al. were again determined via the callibrations of Martins et al., with reddening for individual stars calculated via the intrinsic colours of Martins & Plez (2006). Finally, given their rather evolved nature, we adopted the results of the tailored non-LTE analysis of Crowther & Evans (2009) for HD 151804 and 152408.

Comparison of these data to non-rotating and rotating Geneva isochrones clearly indicate that the region *as a whole* appears non coeval, at first glance being consistent with a spread of ages of between 2.5−5 Myr. Such a conclusion is supported by inspection of the properties of individual stars in both association and cluster, although interpretation is complicated by possible contamination of the latter by the former if, as seems likely, Sco OB1 hosts a younger population than is found in NGC 6231.

A large number of Main Sequence (MS) stars are found within NGC 6231, with the O8 V companion in the binary HD 152234 apparently being the earliest and defining the MS turnoff; consistent with an age of 5 Myr. While an O6 V companion to the WC7 star WR 79 has been reported (Hill et al. 2000) the 126 day binary period of HD 152234 will have ensured that neither component in this system will have interacted, while the 8.89 day period of WR79 indicates that significant mass transfer to the secondary may have occured (e.g. Petrovic et al. 2005). Encouragingly, the O9.7Ia primary of HD 152234 also lies on the 5 Myr isochrone for rapid initial rotation, with the *current v*sin*i* also being consistent with this placement (Fraser et al. 2010).

Building on this approach, we find that HD 152219 (O9.5 III + B1-2 III-V) and HD 152134 (B0.5 Ia) lie upon the 5 Myr evolutionary track for non-rotating stars, with – sequentially – HD 326331 (O8 III((f))), HD 152247 (O9 III), HD 152249 (O9 Ib((f))) and HD 152234 (O9.7 Ia + O8 V) following the rotating track. In both cases the systematic progression to later spectral types with increasing luminosity class suggest these are real evolutionary sequences (cf. Cyg OB2; Negueruela et al. 2008).

However, there are a number of stars within NGC 6231 and Sco OB1 that appear incompatable with a ~5 Myr population: the O8 Iafpe/WN9ha stars HD 151804 and 152048 and the O5.5-7.5 III stars HD 151515, 152723, 152233 and 152248. Regarding the former pair, Bohannan & Crowther (1999) suggest a close physical kinship between these objects, apparently precluding an evolution through the cooler late-O/early-BSG phase present in NGC 6231. Of the mid-O giants, HD 151515 and 152723 appear somewhat subluminous for their spectral type but the properties of the O5.5 III(f) + O7.5 and O7.5 III(f) + O7 III(f) binaries HD 152233 and 152248 (Sana et al. 2008; 2001) clearly support the assertion that a younger population is present; although the dymanical masses for both components of the latter system appear somewhat lower than expected (29.6 $M_{\odot}$ and 29.9 $M_{\odot}$ respectively).

We therefore conclude that comparison of NGC 6231 to Sco OB1 *implies* that the respective stellar populations are non coeval. However, with the exception of HD 152233 and HD 152248, the massive stellar population of NGC6231 appears consistent with a single burst of star formation ~5 Myr ago. Indeed, no early-mid O MS stars consistent with a younger

population appears present within NGC 6231, while the population of late-O/early-B MS stars that are present are systematically displaced redwards from the ≤ 3 Myr isochrones. Therefore, if they *are* members of NGC 6231, we cannot exclude the possibility that, with spectral types <O8, HD 152233 and HD 152248 are in fact bona fide blue stragglers; having evolved via a different pathway from the majority of stars and hence that NGC 6231 is truly coeval. In this respect it would therefore closely resemble Cyg OB2, for which Negueruela et al. (2008) arrived at a comparable conclusion.

Appendix D: Spectral fits to ζ^1 Sco and HD 190603

We present additional model fits to ζ^1 Sco based on the FEROS (3700–8850 Å) optical data (not presented in the paper version due to reasons of space).
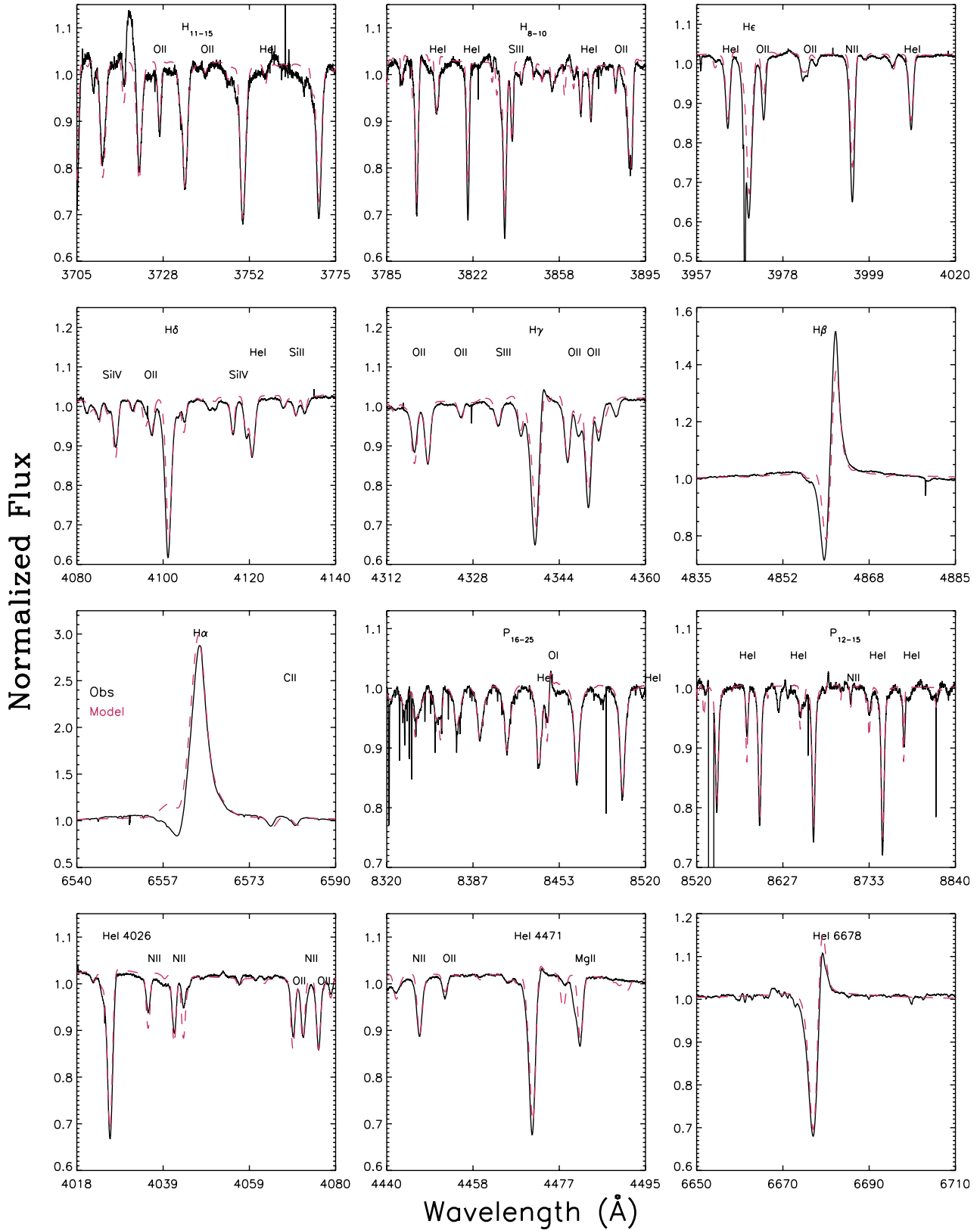
Fig. D.1. Comparison of the synthetic spectrum of ζ^1 Sco (red dashed line) to observational data for various transitions between 4090–22 100 Å. Optical data correspond to the FEROS data kindly provided by Otmar Stahl. Note the lack of long-term variability between these data and those presented in Fig. 7.
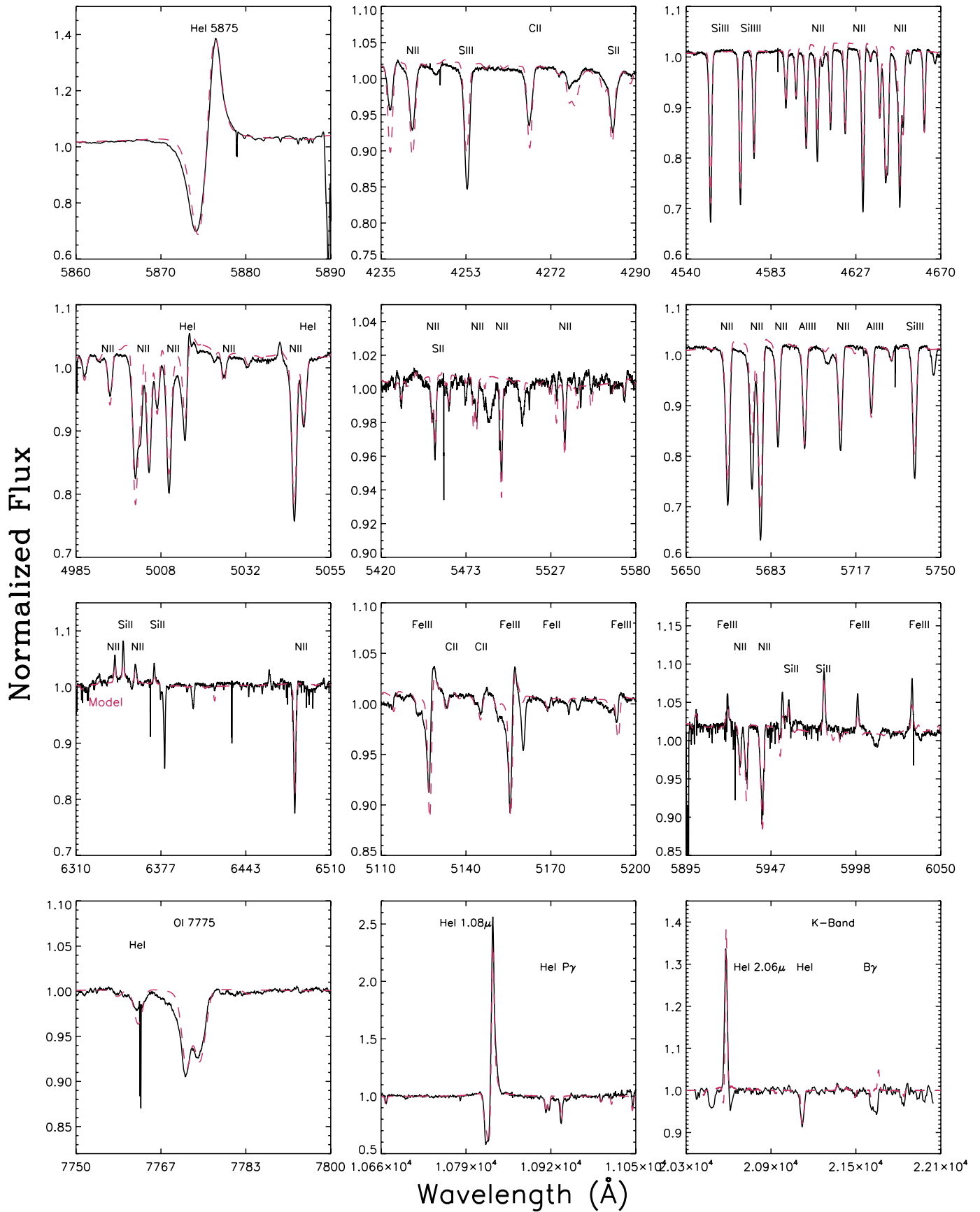
Fig. D.1. continued.